2021

Gq-Mediated Ca** Signals in Human Airway Smooth Muscle Cells

Hanna Viktoria Bobinger
University of South Alabama

2021

Gq-Mediated Ca** Signals in Human Airway Smooth Muscle Cells

Hanna Viktoria Bobinger
University of South Alabama

THE UNIVERSITY OF SOUTH ALABAMA
COLLEGE OF ENGINEERING

G_q-Mediated Ca^{++} Signals in Human Airway Smooth Muscle Cells

BY

Hanna Viktoria Bobinger

A Thesis

Submitted to the Undergraduate Faculty of the
University of South Alabama
in partial fulfillment of the
requirements for the degree of

Bachelor of Science

in

Chemical Engineering

May 2021

Approved: Date:

Thomas Rich 05/03/2021

Co-Chair of Thesis Committee: Dr. Thomas C. Rich

05/04/2021

Co-Chair of Thesis Committee: Dr. Silas J. Leavesley

05/04/2021

Committee Member: Dr. Christopher M. Francis

Sean Walker 05/04/2021

Committee Member: Dr. Sean B. Walker

Dean of the Honors College: Dr. Kathy J. Cooke

G_q-Mediated Calcium Signals in Human Airway Smooth Muscle Cells

A Thesis

Submitted to the Undergraduate Faculty of the
University of South Alabama
in partial fulfillment of the
requirements for the degree of

Bachelor of Science

in

Chemical Engineering

by
Hanna Viktoria Bobinger

May 2021

ACKNOWLEDGEMENTS

First and foremost, I would like to thank my mentors Dr. Thomas C. Rich and Dr. Silas J. Leavesley. As an incoming freshman, you both welcomed me into your laboratory, helped me through two summer research projects, and constantly supported my applications in the pursuance of my career goals. Dr. Rich, I will forever be grateful for giving me the opportunity to work with your colleague, Dr. Pierre Vincent, in Paris, France. The experience was transformative and allowed me to learn from a diverse group of scientists, who I still keep in contact with today. Next, I would like to thank Dr. Naga S. Annamdevula, Dr. DJ Pleshinger, and Santina C. Johnson. You were always ready to provide feedback on my work or further my understanding on data analysis. Without your help, I am sure that the figures in this thesis would not have come to fruition. I would also like to acknowledge Andrea Britain, who taught me how to prepare my cells and walked through countless experiments with me. I would like to thank Dr. Trudy Cornwell for training me to use the Andor WD spinning disk confocal microscope; your guidance increased my confidence to independently run experiments in a lab, and you were always one call away if I needed help. Furthermore, I would like to thank Dr. Sean B. Walker, not only for being a part of my thesis committee, but also for being an encouraging educator in my upper-level chemical engineering courses and for supporting my professional school application. I would like to thank Dr. C. Michael Francis for being a part of my thesis

committee and for assisting with the S8 analysis software. I would like to thank the University of South Alabama (USA) Center for Lung Biology for the use of equipment and facilities, as well as the Office of Undergraduate Research (SURF) for funding. Lastly, I would like to thank my parents and siblings for their continued support through the highs and lows of my undergraduate years.

TABLE OF CONTENTS

Page

LIST OF TABLES

LIST OF FIGURES

Figure Page

Appendix Figure Page

LIST OF SCHEMES

Scheme Page

LIST OF ABBREVIATIONS

β_2-AR: beta 2-adrenergic receptor

ASM: airway smooth muscle

TAS2R: bitter taste 2 receptor

HASMC: human airway smooth muscle cell

Ca^{++}: calcium

m3 mAChR: m3 muscarinic acetylcholine receptor

H1R: histamine 1 receptor

GPCR: G protein-coupled receptor

SABA: short-acting β_2-AR agonist

LABA: long-acting β agonist

LAMA: long-acting muscarinic agonist

SAMA: short-acting muscarinic agonist

AC: adenylyl cyclase

ATP: adenosine triphosphate

cAMP: cyclic adenosine monophosphate

PKA: protein kinase A

PLC: phospholipase C

IP_3: inositol 1,4,5-triphosphate

GDP: guanosine diphosphate

GTP: guanosine-5'-triphosphate

PIP_2: phosphatidylinositol 4,5-bisphosphate

DAG: diacylglycerol

NK_2R: tachykinin receptor

VDCC: voltage-dependent Ca^{++} channel

AM: acetoxymethyl

BAPTA: 1,2-*bis*-(2-aminophenoxy)ethane-N,N,N',N'-tetraacetic acid

SDCLM: spinning disk confocal laser microscopy

ROI: region of interest

DMEM: Dulbecco's Modified Eagle Medium

H_2O: water

FBS: fetal bovine serum

SMC^{TM}: Single Molecule Counting

bFGF: basic fibroblast growth factor

EGF: epidermal growth factor

PBS: phosphate-buffered saline

MW: molecular weight

DMSO: dimethyl sulfoxide

NaCl: sodium chloride

KCl: potassium chloride

HEPES: 2-[4-(2-hydroxyethyl)piperazin-1-yl]ethanesulfonic acid

$MgCl_2$: magnesium chloride

$CaCl_2$: calcium dichloride

dd H_2O: deionized water

Hz: hertz

s: second

TRPV4: transient receptor potential cation channel subfamily V member 4

A.U.: arbitrary units

ABSTRACT

Bobinger, Hanna, Viktoria, B. S., University of South Alabama, May 2021. G_q-Mediated Calcium Signals in Human Airway Smooth Muscle Cells. Co-Chair of Committee: Rich, Thomas, C., Ph.D., Co-Chair of Committee: Leavesley, Silas, J., Ph.D.

Current asthma therapies include corticosteroids, long acting β_2-adrenergic receptor (β_2-AR) agonists paired with corticosteroids, or short-acting β_2-AR agonists used in rescue inhalers. Chronic use of β-agonists results in diminished effectiveness, and use of long-acting β-agonists can even exacerbate asthma symptoms; this is partly because anti-inflammatory therapy does not directly address the exaggerated airway narrowing due to excessive shortening of airway smooth muscle (ASM), which is the hallmark of asthma.[1] These observations led our collaborators to investigate other potential asthma therapies – bitter taste agonists.[2] Bitter taste agonists, such as chloroquine, activate a subset of G_q-coupled receptors known as bitter taste 2 receptors (TAS2Rs) in airway smooth muscle cells. Activation of these receptors triggers relaxation of human airway smooth muscle cells (HASMCs). This response is markedly different than the response to activation of other G_q-coupled receptors, such as muscarinic receptors, which when activated trigger contraction of HASMCs. The goal of this thesis project is to understand how different G_q-coupled receptor agonists trigger distinct responses in HASMCs. The working hypothesis is that differences in the spatial distributions and/or kinetics (duration) of intracellular calcium (Ca^{++}) signals are responsible for the distinct responses. To test this hypothesis,

HASMCs were treated with different concentrations of carbachol (1 – 50 μM), a m3 muscarinic acetylcholine receptor (m3 mAChR) agonist; chloroquine (10 – 200 μM), a TAS2R agonist; or histamine (0.5 – 5 μM), a histamine 1 receptor (H1R) agonist, to target different subsets of G_q-mediated receptors. HASMCs were loaded with Cal-520® AM, a green-fluorescent dye that, upon binding to intracellular Ca^{++}, increases its fluorescence intensity. Change in intracellular Ca^{++} following agonist addition were visualized and measured over time using an Andor WD spinning disk confocal microscope. Distinct spatial differences in Ca^{++} signals in response the agonist addition were quantified by measuring two parameters – Ca^{++} signal maximum intensity in the identified signal areas over time and Ca^{++} signal area changes over time. Distinct kinetic differences in Ca^{++} signals were quantified by measuring two more parameters: Ca^{++} signal duration and the number of identified Ca^{++} responses induced by each agonist per experiment. Furthermore, the distinct changes in peak intensity, signal area, duration, and number of induced Ca^{++} signals were analyzed for possible concentration dependencies, which could provide future insight into the unique airway responses induced by each agonist.

INTRODUCTION

Second messenger signals, including Ca^{++} signals, simultaneously orchestrate dozens of cellular functions. They have been the subject of extensive study for the last 70 years. However, the mechanisms underlying specificity in signal transduction pathways remain unclear. Increases in intracellular Ca^{++} have historically been known to induce ASM contraction, leading to constriction of the airways. One class of G protein-coupled receptors (GPCRs), G_q-coupled receptors, regulates increases in intracellular Ca^{++} upon binding of an endogenous ligand or exogenous agonist. However, activation of a particular subset of G_q-coupled receptors, TAS2Rs, paradoxically induces ASM relaxation despite causing increases in intracellular Ca^{++}.[3] This unique downstream effect, despite an increase in cytosolic Ca^{++} via the same pathway, underscores the integral role of second-messenger (e.g. Ca^{++}) specificity in determining critical cellular functions via the G_q-coupled receptor signal transduction pathway. Specifically, this observation by Conaway, Nayak, and Deshpande highlights the importance of understanding how differences in the spatial and kinetic distributions of intracellular Ca^{++} signals contribute to distinct airway responses.

In general, signaling through GPCRs plays an integral role in determining airway response upon binding of an agonist or ligand. GPCRs are ubiquitously-expressed receptors that contain 7 membrane-spanning α-helices, which are separated by alternating intracellular and extracellular regions.[4] There are almost 1,000 different types of GPCRs

found in the human genome, which are specific to particular agonists.[5] When an agonist binds to a GPCR, the heterotrimeric G protein associated with that receptor is activated. The G protein is called heterotrimeric because it has three different subunits (α, β, and γ). In general, there are four subfamilies of GPCRs (G_s, $G_{i/o}$, G_q, and $G_{12/13}$) based on the type of G protein that the receptor interacts with, and all four subfamilies are expressed in HASMCs.[6] Each subfamily is classified by the different type of α subunit composed in its G protein that is activated and involved in signal transduction.[6] The class of GPCRs expressed on HASMCs that will be studied in the context of airway relaxation or constriction are G_q-coupled GPCRs, specifically TAS2Rs, H1Rs, and m3 mAChRs. For reference, all three of the aforementioned receptors are further coupled to different subsets of G_q-coupled receptors. For example, TAS2Rs are associated with the gustducin G_q α subunit.[7]

CHAPTER I: CURRENT ASTHMA THERAPIES

Asthma is characterized by excessive narrowing of airways in response to specific or non-specific stimuli, and ASM is primarily responsible for this narrowing.[8] The majority of current asthma treatments directly target GPCRs or their downstream signals, including the β_2-AR, which is coupled to the G_s α subunit.[6] β-adrenergic agonists, such as epinephrine (the first bronchodilator) and isoprenaline derivatives, are used today in rescue and maintenance inhalers for asthmatic patients.[9] Currently, inhaled short-acting β_2-AR agonists (SABAs), such as albuterol, are the first treatment of choice during acute asthma attacks as they are the most potent bronchodilators that have been approved.[6,10] SABAs are also widely used as the second line of defense to manage chronic asthma symptoms, such as airway narrowing, because they are historically known to relax their principal target – ASM. Long-acting β-agonists (LABAs), such as salmeterol and formoterol, have longer half-lives upon binding to β_2-ARs and offer symptomatic relief of chronic asthma.[10] Furthermore, LABAs utilized in combination with inhaled corticosteroids are the first line of defense in controlling chronic asthma symptoms. Evidence suggests that this combination therapy enhances the anti-inflammatory effects that either drug could achieve individually.[11] One specific combination includes formoterol/budesonide due to its quick onset of action.[10] Beyond inhaled corticosteroids, LABAs, and SABAs, long-acting muscarinic antagonists (LAMAs) and short-acting muscarinic antagonists (SAMAs) are

also currently available, third- or fourth-line chronic asthma treatment options. They are utilized for asthmatics for whom LABAs and SABAs are insufficient. LAMAs include tiotropium and ipratropium, which are G_q-coupled receptor antagonists that bind to muscarinic receptors M1, M2 and M3 to block acetylcholine (a G_q receptor contractile agonist), leading to decreases in bronchoconstriction. However, only tiotropium has received approval for use in managing asthma, whereas other LAMAs are currently used in the treatment of chronic obstructive pulmonary disease and have yet to be developed and approved as asthma drugs.[10]

SABAs and LABAs exhibit similar mechanisms of actions albeit with varying durations of action. Once a SABA or LABA binds to the β_2AR, the receptor undergoes a conformational change, and the G_s α subunit is activated. Upon activation, the α subunit binds to and activates adenylyl cyclase (AC), which is bound to the membrane. Activated AC utilizes adenosine triphosphate (ATP) from the cytoplasm to form cyclic adenosine monophosphate (cAMP), which is a second messenger signal. cAMP's principal function is to activate protein kinase A (PKA) because cAMP has a high binding affinity for domains in PKA's regulatory region. Activated PKA subsequently phosphorylates certain G_q-coupled receptors and phospholipase C (PLC), inhibiting Ca^{++} flux, which has historically been known to trigger ASM contraction. PKA also phosphorylates inositol 1,4,5-triphosphate (IP_3) receptors, thereby reducing transport of Ca^{++} into the cytoplasm from IP_3-specific stores. Furthermore, PKA phosphorylates myosin light chain kinase to decrease its affinity to calcium-calmodulin, which reduces myosin light chain phosphorylation that would otherwise allow for ASM contraction.[6]

However, the common combination of β-adrenergic agonists and corticosteroids is not effective in long-term control of asthmatic symptoms.[9] Studies have indicated associations between inhaled or oral β_2-AR agonists and an increased risk of cardiovascular death, ischemic heart disease, and cardiac failure.[12] Furthermore, SABAs have been shown to cause airway hyperresponsiveness to specific and non-specific stimuli, leading to increased airway inflammation.[13] Moreover, when asthmatics contract infections, such as influenza or pneumonia, rescue inhalers are less effective at inducing airway relaxation. Because the combination of β-adrenergic agonists and corticosteroids is not effective in long-term control of asthma-related symptoms[9], alternative or complementary strategies for the treatment of asthma are currently being explored.

CHAPTER II: G_q-COUPLED RECEPTORS

2.1 G_q-Coupled Ca^{++} Signal Transduction Pathway

Historically, G_q-coupled receptors have been known as the principal mediators of ASM contraction.[6] However, bitter taste receptor agonists, which also activate G_q-coupled receptors, offer alternative pathways to achieve ASM relaxation. Activation of bitter taste receptors with bitter taste receptor agonists, such as chloroquine, has been shown to achieve relaxation of HASMCs[2]; this is in stark contrast to other G_q-coupled receptor agonists, such as histamine and carbachol, which trigger HASMC contraction (Figure 1[14]).[6] Originally, it was thought that bitter taste receptors were expressed on human ASM as avoidance receptors for toxic inhalants, leading to contraction of the airways.[2] Although bitter taste agonists follow the same signal transduction pathway as contractile G_q agonists, differences in their intracellular Ca^{++}-induced signals may explain the different airway responses observed. Furthermore, bitter taste agonists offer the potential to address the aforementioned shortcomings of current asthma therapies. Specifically, current therapies do not address progressive airway remodeling. Bitter taste agonists not only induce bronchodilatory effects but also inhibit allergen-induced inflammatory responses, regulate ASM cell proliferation, and reduce airway remodeling.[11] Furthermore, it was observed that

bitter taste agonists induce a 3-fold greater dilation of airways than β-agonists in an asthma mouse model.[2] Therefore, bitter taste agonists are currently being explored for future

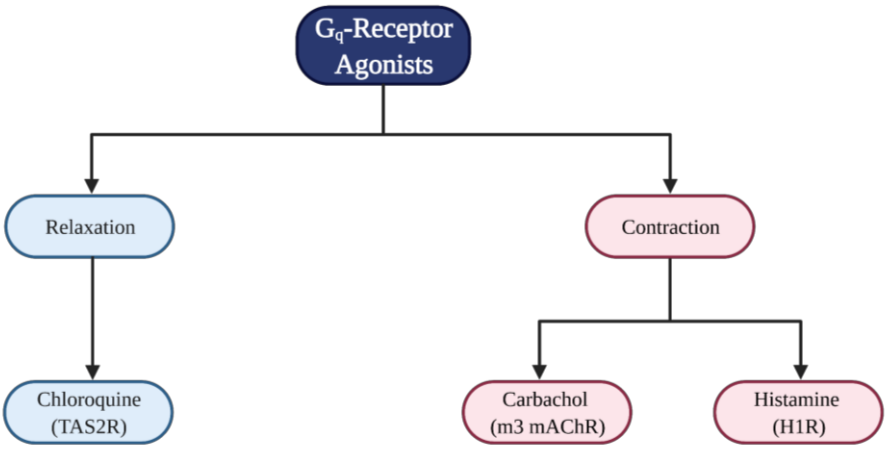

Figure 1.[14] Subsets of G_q-coupled receptors responsible for distinct airway responses upon binding of specific agonists.

implementation as alternative or add-on therapies to address the shortcomings of current asthma treatments.

It is hypothesized that the induced intracellular Ca^{++} signal location and kinetics are responsible for the distinct responses of ASM to activation of various G_q-coupled receptors, thus leading to either relaxation or constriction of airways. To understand these differences, the GPCR signaling pathway for G_q-coupled receptors must first be understood.

G_q protein-coupled receptors transduce a second-messenger signal (e.g. Ca^{++}) to the interior of cells via interactions with guanine nucleotide regulatory binding proteins.[9] In general, when a ligand or agonist extracellularly binds to and activates a GPCR, the GPCR undergoes a conformational change and exposes a high-affinity binding site for a G protein in its guanosine diphosphate (GDP)-bound inactive state. Specifically, the receptor

interacts with the C-terminus of the α subunit of a membrane-bound, heterotrimeric, inactive G protein, such as G_q. This binding or coupling of a G protein to a GPCR releases GDP and thus creates an empty nucleotide binding pocket for guanosine-5'-triphosphate (GTP); GTP exists at a higher concentration than GDP in the cytosol. Binding of GTP causes the dissociation of the α subunit from the $G_{\beta\gamma}$ dimer and activates the G protein. Once the G protein is activated, because the γ subunit is still bound to GTP, the G protein's effector domain is exposed, activating PLC. PLC promotes hydrolysis of phosphatidylinositol 4,5-bisphosphate (PIP_2) into intracellular messengers diacylglycerol (DAG) and IP_3. IP_3 subsequently translocates and binds to IP_3 receptors located on sarcoplasmic reticulum Ca^{++} stores. Activating the IP_3 receptors opens Ca^{++} channels, and Ca^{++} can efflux into the cytosol. This increase in intracellular Ca^{++} is a major source of Ca^{++}'s role in ASM contraction.[6] The goal of this work is to identify how agonists targeting different G_q receptors, despite triggering the same G_q protein signal transduction pathway, may lead to spatial and kinetic (duration) differences in Ca^{++} gradients, ultimately determining if ASM will relax or contract.

While the G_s-coupled β_2-AR signaling cascade induces ASM relaxation in response to a β_2-agonist, historically, signaling via G_q-coupled receptors in ASM has promoted ASM contraction with transmembrane cascades that occur via the classic G_q pathway (Figure 2). For example, the H1R is a G_q-coupled receptor capable of inducing significant ASM contraction in vivo or ex vivo.[6]

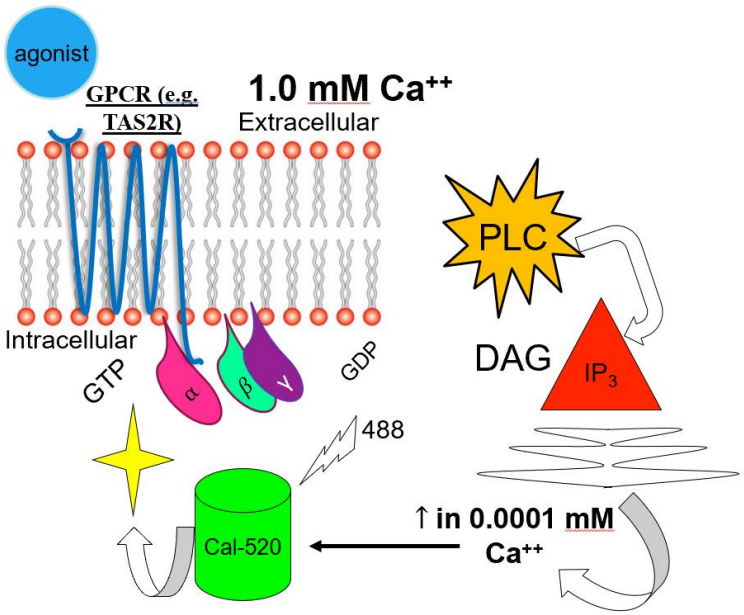

Figure 2. G_q GPCR Ca^{++} signal transduction pathway. G_q receptors binding an agonist can activate a signal transduction pathway to ultimately increase intracellular Ca^{++} concentration. IP_3 and DAG are generated from PLC activation, leading to activation of IP_3 receptors in the sarcoplasmic reticulum, which triggers release of Ca^{++}. Ca^{++} can then bind to the Cal-520® AM fluorescent sensor in the cytoplasm, which increases its fluorescence, indicating increases in intracellular Ca^{++}.

2.2 Maintaining ASM Tone (The Contractile State) and Aberrant GPCR Signaling

ASM contractile state is a function of the net sum of GPCR-mediated pro-contractile and pro-relaxant signals which ultimately establish the level of Ca^{++}, the key contractile signaling molecule, in the ASM cell. Additionally, the ASM contractile state is a function of the cell's contractile machinery response to Ca^{++}. Furthermore, ASM is innervated by postganglionic parasympathetic nerves releasing acetylcholine in order to control resting ASM tone, and activation of specific GPCRs in ASM has a direct impact on the contractile state of ASM.[6] The m3 mAChR, which the agonist carbachol binds to, also maintains the contractile state of ASM, known as maintaining ASM "tone".[6]

Changes in maintenance of the ASM contractile state are the primary causes of increased airway resistance, which is a defining feature of asthma, and thus a cause of exacerbation of symptoms after long-term use of β-agonists.[6] The asthmatic airway is unable to properly maintain the ASM contractile state due in part to aberrant GPCR signaling in ASM, which contributes to elevated ASM tone. The normal GPCR signaling pathway that induces ASM contraction establishes the level of Ca^{++} in the ASM cell and may be altered at three different levels in the asthmatic airway (Figure 3).[6] On the first level, HASMCs could be exposed to a greater concentration of agonists targeting G_q-coupled receptors, which generally promote contraction, and/or a decreased concentration of agonists that promote ASM relaxation by targeting G_s-coupled receptors. Furthermore, stimulation of ASM with multiple contractile G_q-coupled receptor agonists has been shown to have a synergistic effect on contraction, further exacerbating the elevated ASM tone.[15] This increased or decreased access of pro-contractile and pro-relaxant agonists, respectively, may be linked to the increased shedding of airway epithelium in the asthmatic airway. On the second level, G_q-coupled receptor signaling may be hypersensitized, or G_s-coupled receptor signaling may be desensitized, which promotes increased PIP_2 hydrolysis and thus increased intracellular Ca^{++} mobilization. Lastly, on the third level, the cell's contractile response to Ca^{++} may be exaggerated due to increased myosin light chain phosphorylation.

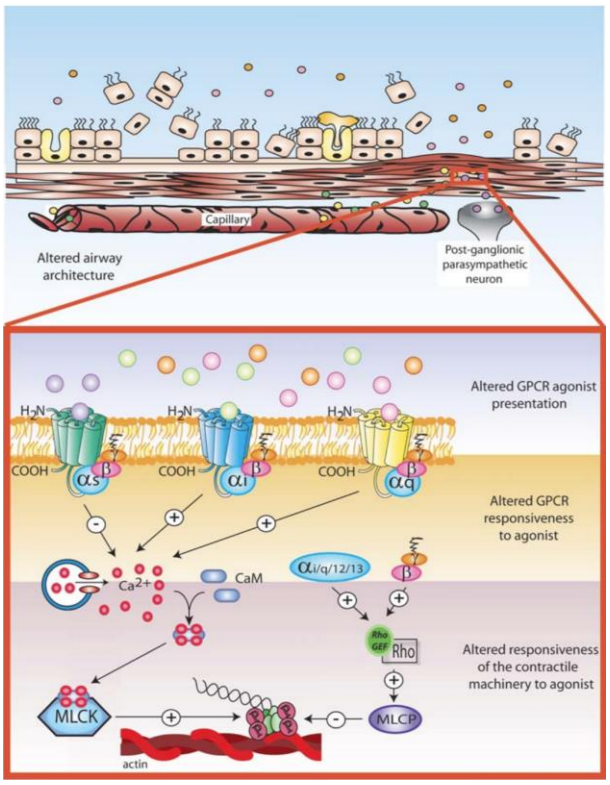

Figure 3. Aberrant GPCR signaling in ASM.[6] Alteration of the normal GPCR signaling pathway in ASM can occur at three different points in the asthmatic airway, ultimately leading to elevated ASM tone.

It has specifically been shown that long-term β-agonist therapy, one of the most widely used drug therapies in the treatment of asthma, affects the second level (receptor expression and coupling) of the GPCR signaling pathway in ASM. Long-term β-agonist therapy promotes the sensitization of pro-contractile GPCR signaling and desensitization of pro-relaxant GPCR signaling, exacerbating bronchial hyperresponsiveness in asthmatics. Mak et al. have demonstrated that exposure of ASM ex vivo to β-agonists up-regulates both tachykinin (NK_2)[16] and H1 receptors[17], which could be connected to a mechanism whereby increased pro-contractile GPCR signaling promotes bronchial hyperresponsiveness.

It is worth noting that while ASM cultures (ex vivo) are powerful experimental models due to the fact that ASM cells in culture maintain physiologic levels of most signaling components (receptors, effectors, and downstream signaling intermediates), the model's weak point lies in the decreased expression of G_q-coupled receptors such as the m3 mAChR.[6]

Since it has recently been discovered that activation of G_q-coupled TAS2Rs with bitter taste receptor agonists, such as chloroquine, triggers relaxation of HASMCs by localized Ca^{++} signaling[2], further investigation is warranted into the role of Ca^{++} signal location or kinetics (duration) in the relaxation or contraction of ASM.

CHAPTER III: CHARACTERISTICS OF CA^{++} SIGNALING

3.1 Ca^{++} Influx from the Extracellular Environment

While activation of G_q-coupled receptors induces increases in intracellular Ca^{++} as detailed previously, the major contributors to increases in intracellular Ca^{++} are voltage-dependent Ca^{++} channels (VDCCs). Activation or opening of VDCCs is primarily sensitive to changes in voltage or exogenous, pharmacological Ca^{++} channel blockers. VDCCs can mediate different types of Ca^{++} signals such as global increases in intracellular Ca^{++}, Ca^{++} flashes, and Ca^{++} "sparklets."[18] In smooth muscle cells, depolarization of the membrane from its resting potential can lead to ubiquitous elevations in Ca^{++}, whereas hyperpolarization lowers the concentration of intracellular Ca^{++}. Similarly, smooth muscle can also exhibit action potentials, or transient changes in membrane potential which allow Ca^{++} entry through VDCCs into ASM cells. This transient, rapid increase in global intracellular Ca^{++} concentration is visualized as a Ca^{++} flash. Ca^{++} flashes can be initiated by the spontaneous release of endogenous ligands. On the other hand, localized Ca^{++} signals caused by the opening of a VDCC are referred to as Ca^{++} sparklets, as opposed to the global Ca^{++} flashes. Ca^{++} sparklets are mostly stationary events that occur in specific regions.[18]

3.2 Ca^{++} Signal Compartmentalization (Ca^{++} Sparks)

Because we sought to identify and characterize the spatial and temporal differences in agonist-induced Ca^{++} signals in HASMCs, it is important to note that localized intracellular Ca^{++} signals can manifest as Ca^{++} sparks (puffs) or waves. In general, smooth muscle cells form a continuous layer and are found in the walls of hollow organs such as the airways; therefore, they are integral in regulating the contraction of functional organs. As noted earlier, specifically in the context of airway contraction, hollow organ function is regulated by changes in intracellular Ca^{++} concentration. However, these concentration changes can manifest in a variety of ways, both spatially and temporally. According to Hill-Eubanks, Werner, Heppner, and Nelson, Ca^{++} changes may be transient or prolonged and may be stationary, propagating, or oscillatory.[18] Increases in intracellular Ca^{++} usually originate from Ca^{++} stores in the sarcoplasmic reticulum. Once an agonist binds to a G_q-coupled receptor, PIP_2 is hydrolyzed, and one of the products of hydrolysis is IP_3. Therefore, the intracellular concentration of IP_3 increases, and IP_3 binds to IP_3 receptors. As mentioned previously, when IP_3 binds to specific IP_3 receptors in the sarcoplasmic reticulum upon initiation of the G_q signaling pathway, activated IP_3 receptors release Ca^{++} from stores in the sarcoplasmic reticulum into the cytosol, leading to characteristic Ca^{++} signals.[18] Moreover, Ca^{++} release from IP_3 receptors can lead to Ca^{++}-induced Ca^{++} release. According to Hill-Eubanks et al., Ca^{++} released by activated IP_3 receptors is regulated by IP_3 and Ca^{++}, both functioning as second messengers. Released Ca^{++} can aggregate in higher-concentration (low micromolar) levels in the vicinity of the Ca^{++} channel, once again activating IP_3 receptors. At even higher concentrations outside the IP_3 receptors, the

channel becomes inactivated, thus contributing to a variety of spatially and kinetically unique Ca^{++} signals. Furthermore, according to Hill-Eubanks et al., IP_3 receptor-mediated Ca^{++} release is transient and localized, known as Ca^{++} "sparks" or "puffs." Ca^{++} puffs can subsequently lead to intracellular Ca^{++} waves.

Ca^{++} waves, on the other hand, are increases in intracellular Ca^{++} that propagate across the entire smooth muscle cell area (i.e. non-localized) from an initial origination point.[18] As Ca^{++} that is released from the sarcoplasmic reticulum acts on individual adjacent IP_3 receptors or IP_3 receptor clusters, the signals cascade along these receptors. These waves are maintained by continuously restoring Ca^{++} to its stores in the sarcoplasmic reticulum and subsequently releasing it again.

CHAPTER IV: FLUORESCENCE MICROSCOPY

4.1 Ca^{++} Fluorescent Dye: Cal-520® AM

Ca^{++}-sensitive fluorescent dyes allow the quantitative measurement of changes in intracellular Ca^{++} levels in cells. Fluorescent dyes can absorb specific wavelengths of light and release energy in the form of light at longer wavelengths. When Ca^{++} binds to Ca^{++}-sensitive indicators, the fluorescence properties of the indicators change. Recent developments of fluorescent dyes enable the detection of rapid Ca^{++} signal changes, even within milliseconds. Fluorescent dyes are commonly loaded into cells via incubation with the membrane-permeant acetoxymethyl (AM) ester form of the dye, which is attached to a fluorophore. The AM form can readily pass through the cell's plasma membrane. Once the AM form is inside the cell, intracellular esterases cleave the ester bond to release the free anion (negative charge), which cannot pass through the plasma membrane and thus stays inside the cell to bind to Ca^{++}. Fluorescent Ca^{++} indicators are usually derivatives of the Ca^{++} chelator, namely 1,2-*bis*-(2-aminophenoxy)ethane-N,N,N',N'-tetraacetic acid (BAPTA), which is used for ratiometric and nonratiometric Ca^{++} measurements. Nonratiometric dyes show increases in fluorescence intensity by binding intracellular Ca^{++}.[18] Fluorescent Ca^{++} signal indicators were originally developed by Roger Tsien.[19] According to Tsien, BAPTA and its derivatives are ideal as they are not significantly affected by pH changes.[20] This means that BAPTA derivatives such as Cal-520® are less

sensitive to the loading conditions, thereby decreasing variability between experiments. In low-concentration environments of Ca^{++}, once the dye is excited by a laser, induced electron transfer from the Ca^{++} chelator inhibits fluorescence of the fluorophore. When intracellular Ca^{++} concentration increases, this electron transfer is blocked, subsequently resulting in changes in fluorescence intensity. Fura-2 was the first commonly used Ca^{++} indicator and was a ratiometric probe, meaning it required excitation by wavelengths in the UV region of light, which proves toxic to cells. Thus, single wavelength Ca^{++} indicators, such as Fluo-4, were developed to bind intracellular Ca^{++} and are utilized to study rapid intracellular Ca^{++} intensity gradients. These single wavelength Ca^{++} indicators operate within the visible light spectrum, usually requiring blue excitation wavelengths and emitting at green wavelengths.[19] According to Lock, Parker, and Smith, Cal-520® is the optimal Ca^{++} fluorescent indicator for detecting and measuring local Ca^{++} changes over time.[19] Changes in the Cal-520® probe intensity directly indicate changes in intracellular Ca^{++} concentration.

4.2 Spinning Disk Confocal Microscopy

To determine how spatial and kinetic differences of Ca^{++} signals contribute to airway relaxation or constriction, differences in global or localized Ca^{++} signals must be measured at high speeds. In other words, characterization of dynamic intracellular Ca^{++} signals requires high temporal and spatial resolution. Spinning disk confocal laser microscopy (SDCLM) helps to overcome this hurdle. SDCLM illuminates samples with rotating patterns of thousands of pinholes to completely illuminate all points on the sample simultaneously. Traditional imaging techniques include confocal laser scanning microscopy, where a tradeoff between image resolution and speed exists because the laser

beam must scan each point separately to generate an image. On the other hand, SDCLM utilizes an expanded beam to illuminate an array of lenses on the collector disk. Each lens is associated with a pinhole on the pinhole disk, where both disks are fixed to a common shaft and separated by the focal length of the lens. Exciting the sample while simultaneously spinning both disks allows an array of focused laser beams to be scanned across the sample. This allows in-focus fluorescence emission light to pass through the pinhole disks and be reflected into the camera by a dichroic mirror. Ultimately, low-noise images are achieved with SDCLM.[21]

4.3 S8 Analysis of Ca^{++} Signals

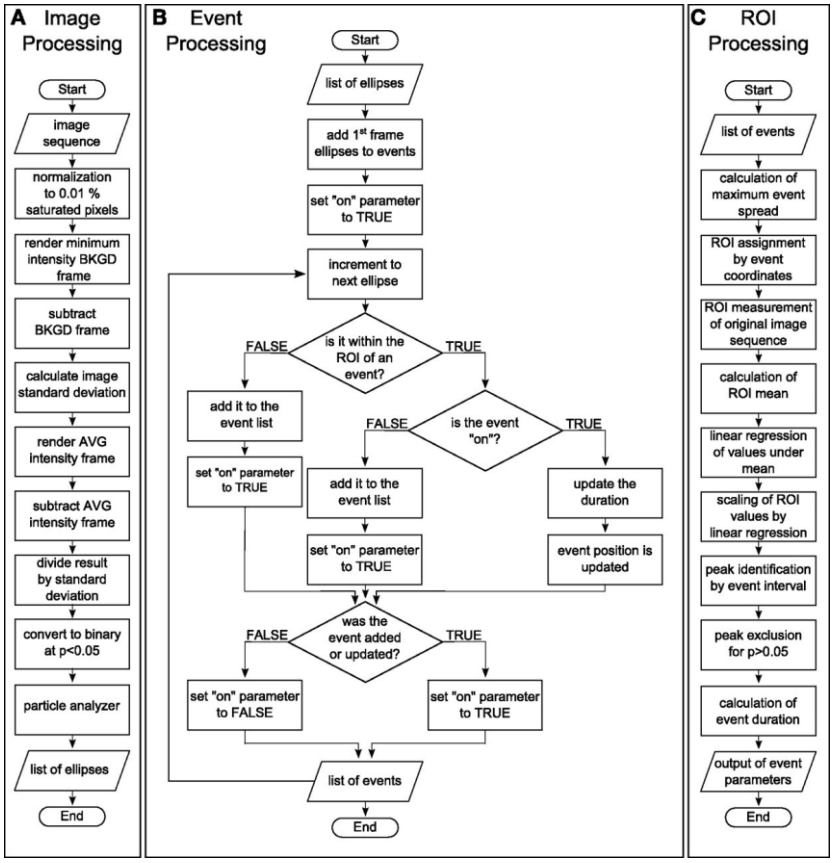

Scheme 1. Signal flow charts of S8 algorithm processes.[22]

The S8 analysis process can be divided into two procedures, statistical noise filtering and analysis of best-fit ellipses assigned to the areas of increased Ca^{++} signal intensities. The latter can subsequently be organized into three subroutines: image processing (A), event processing (B), and region of interest (ROI) processing (C), as illustrated in Scheme 1.

The input to the S8 analysis software is a tiff stack (image sequence), which the algorithm converts into a series of best-fit ellipses using a calculated threshold. Next, the event processing subroutine determines the optimum ROI position. The minimum criteria

to define an "event" are that the ellipses in each event must have an area greater than or equal to a circle of 2-pixel radius and appear in at least two consecutive frames. The event processing subroutine organizes the filtered ellipse locations into ROIs over time and assigns an ROI at the position of each event, which captures the change in signal area over time. Lastly, the mean intensity measurements are computed in each ROI over time, and pre-selected statistical parameters for each pixel and ROI are calculated by the ROI processing subroutine to generate the final outputs desired by the user.[22] Historically, users subjectively defined ROIs based on perceived areas of significant fluorescence intensity fluctuations, and the mean intensity of all the pixels in each ROI was measured over time. However, S8 applies a thresholding method to filter out noise from acquired two-dimensional time lapse image sequences. This project utilized the Otsu thresholding method. Ultimately, this noise filter allows S8 to rapidly assign best-fit ellipses to all elevated Ca^{++} signals above the calculated noise threshold. S8 subsequently measures signal parameters, such as the maximum intensity of a localized Ca^{++} signal, for each disparate pixel and then averages these intensities for each identified ROI over time.

Further improvements to S8 allowed the measurement of signal areas over time, as well as the identification of average signal duration and number of identified responses. In short, S8 enables a more efficient and complete characterization of physiologic Ca^{++}-dependent signaling, capturing its spatial and temporal complexities. By analyzing periodic, localized, and oscillating Ca^{++} signals, S8 paves the way for understanding how diverse Ca^{++} distributions in response to various agonists underlie the regulation of physiological processes. In this case, the four parameters of Ca^{++} signal maximum intensity, Ca^{++} signal area, signal duration, and number of identified responses were

utilized to quantify the spatial and temporal distributions of Ca^{++} signals in response to 3 G_q-coupled receptor agonists.

CHAPTER V: EXPERIMENTAL METHODS

5.1 Cell Culture

HASMCs (cell line N120212 donor) were provided from Dr. Raymond Penn's laboratory at Thomas Jefferson University.

5.1.1 Cell Growth Media Recipe: 1.1 DMEM with 5% FBS

1 packet of DMEM (high glucose; Gibco #11965-092) was added to 900 ml of MilliQ H_2O to achieve a 10% FBS media. 50 ml of FBS (Sigma F6178) was added into a 0.22 μm filter. SMC^{TM} Growth Factors bFGF (human) and EGF (human) were subsequently added to the media. Specifically, 0.5 μg of bFGF (Sigma F0291-25ug) and 2 μg EGF (Invitrogen PHG0311) were added, both per 1 L of media.

5.1.2 Cell Maintenance

1X sterile PBS (Gibco 10010-023) was prewarmed to 37°C. The aforementioned growth media (Experimental Methods Section 5.1.1) was also prewarmed to 37°C. Additionally, 0.25% Trypsin-EDTA (Gibco 25200-056) was prewarmed to 37°C. Media was aspirated from the tissue culture vessel, and the prewarmed PBS was gently added to the vessel. The vessel was tilted to ensure that the FBS serum was completely rinsed using PBS to avoid inhibition of Trypsin by FBS in the following step. PBS was then aspirated from the vessel. The prewarmed 0.25% Trypsin-EDTA was added to the vessel to

thoroughly cover the cells to facilitate detachment of cells from the vessel and disturb cell-to-cell adhesions. Cells were subsequently incubated with Trypsin at 37°C for approximately 5 minutes. The vessel was then tapped to dislodge any cells; cells were checked to be rounded and dislodged from the vessel using the microscope. Prewarmed, fresh media was then added to the vessel, and any cell clumps were diffused with up-and-down pipetting and rinsed to the bottom of the tilted vessel. The cell suspension was then transferred to a 50-ml centrifuge tube and centrifuged for 3 to 5 minutes at 0.5X speed. The media was aspirated from the cell pellet in the tube, and the pellet was resuspended in the appropriate volume of prewarmed, fresh media. Cells were subsequently counted so that they could be added into wells for experiments. An equal volume of cell suspension and 0.4% Trypan Blue stain (Gibco 15250-061), ~20 – 50 µL of each, were mixed into a microfuge tube. 10 µL of the cell/blue mix was loaded into each side of a Countess slide. Cells were then counted on the Countess Counter (Invitrogen). The volume needed for each well was then calculated and subsequently added to the experimental wells containing 25 mm laminin-coated glass cover slips. 1 ml of the cell suspension was added to previously prepared tissue culture vessels with prewarmed, fresh media, if needed for future experimental wells. These vessels were placed in the incubator until further use. Cells with ~90% confluency that were previously added into experimental wells were then utilized for imaging.

5.1.3 Cal-520® AM Loading Protocol[23]

To visualize intracellular Ca^{++} signals when excited with a 488 nm laser, cells were loaded with 10 µM Cal-520® AM (AAT Bioquest 21130, MW = 1102.95 g/mol, Stock =

50 μg) fluorescent indicator dye. Specifically, a 5 mM stock solution of Cal-520® AM was prepared in DMSO. 2 μL of the stock solution was added to the working solution (500 ml buffer + 500 ml medium), yielding a 10 μM final solution. Old medium was removed from the well, and all of the working dye solution was added to the well. The well was subsequently incubated for 45 – 60 minutes at 37°C and assayed within 4 hours. All experiments were conducted at room temperature, 20 – 22°C.

5.1.4 Cover Slip and Agonist Preparation

Cells were washed and assayed in an extracellular Tyrodes 1X buffer (pH = 7.3) containing (mM): 145 NaCl, 4 KCl, 10 HEPES, 10 D-Glucose, 1 $MgCl_2$, and 1 $CaCl_2$ to mimic physiological conditions. Varying concentrations of chloroquine (Sigma C6628, MW = 515.9 g/mol, Stock = 200 nM in dd H_2O), histamine (Sigma H7125 MW = 111.15 g/mol, Stock = 1 M in dd H_2O), or carbachol (Calbiochem 212385, MW = 147.20 g/mol, Stock = 10 mM in DMSO) were prepared to target contractile vs. relaxant G_q-coupled receptors. Carbachol treatments were left on ice until added to the cover slip, as required by the DMSO solvent. Cover slips were transferred to an Attofluor^{TM} with the Tyrodes 1X buffer prior to imaging.

5.2 Revolution Andor WD Spinning Disk Confocal Microscope Image Procedure

Raw images were taken on a Revolution Andor WD spinning disk confocal microscope in an ND2 format outputted by the Nikon Elements software. Images were acquired using a 20X magnification air objective. Bound Ca^{++} was detected by exciting the Cal-520® AM dye with a solid-state laser at 488 nm and collecting emitted fluorescence

above 510 nm. The exposure time was set to 200 ms, and the laser power was set to 15%. Images were acquired at an acquisition frame rate of 1.0 Hertz (Hz) or 1 frame per second (s). Each frame was therefore assumed to correlate to one second or time point, given the negligible time for mechanical opening and closing of the shutter between image captures. A 15-minute (900-s) experiment time lapse yielded ~900 frames per experiment. After acquiring baseline images for 5 minutes, varying concentrations of carbachol, chloroquine, or histamine were added to the cover slip to stimulate increases in intracellular Ca^{++}. The two-dimensional raw images were subsequently converted into individual tiff files using ImageJ. ImageJ was then used to combine the individual tiff files into a 16-bit image stack to input into the S8 analysis software.

5.3 S8 Image Analysis Software

To accurately measure dynamic, agonist-induced intracellular Ca^{++} signals using fluorescent Ca^{++} indicators and microscopy techniques, an automated ROI algorithm named "S8" was employed.[22] Inputs to the S8 software are two-dimensional (x-y space and time) images that are in the tiff stack format (Figure 6) and are taken on a Revolution Andor WD spinning disk confocal microscope. Each x-y frame is approximately associated with one time point at the sampling rate of 1.0 Hz, and an image stack is created using the ImageJ software[24] by combining all x-y images in order to track signals over time. S8 allows for novel, automated identification of ROIs with Ca^{++} signals above the set threshold; this automated identification eliminates user biases and saves time when selecting ROIs. The novel S8 software was written in Python and developed in-house at the USA College of Medicine.

For a given experiment, individual ROIs in a stack were selected in an automated (unbiased) manner if the average intensity of the Ca^{++} signal in a region met a certain threshold. For this project, the Otsu thresholding method was applied to all experimental data, and thresholding values were determined by setting Gaussian values. Once all ROIs were selected by the S8 code, S8 not only measured the maximum intensity of the signals over time (Figure 4), but also tracked how the ROI area increased or decreased over time (Figure 5). Baseline amplitude (intensity) values were computed from pre-treatment intervals (in this case, before 300 s). Intensity measurements were then scaled to fold change (F/F_0) and converted from frames to seconds by an acquisitioned frame rate. In this case, the acquisitioned frame or sampling rate of 1.0 Hz was directly mapped to 1 frame per s, since mechanical opening and closing of the camera shutter between images was considered negligible. S8 identified maximum amplitudes (intensities) for each ROI for each time point. Signal area for each ROI at each time point was computed using a right-side Riemann sum for the maximum intensity over time curve. The S8 code outputs include a stack of processed images in tiff format which are background subtracted and noise filtered, a pdf report, and a pickle file containing quantitative measurements of the four measured signaling parameters over time: maximum signal intensity, signal area, signal duration, and number of identified ROIs.

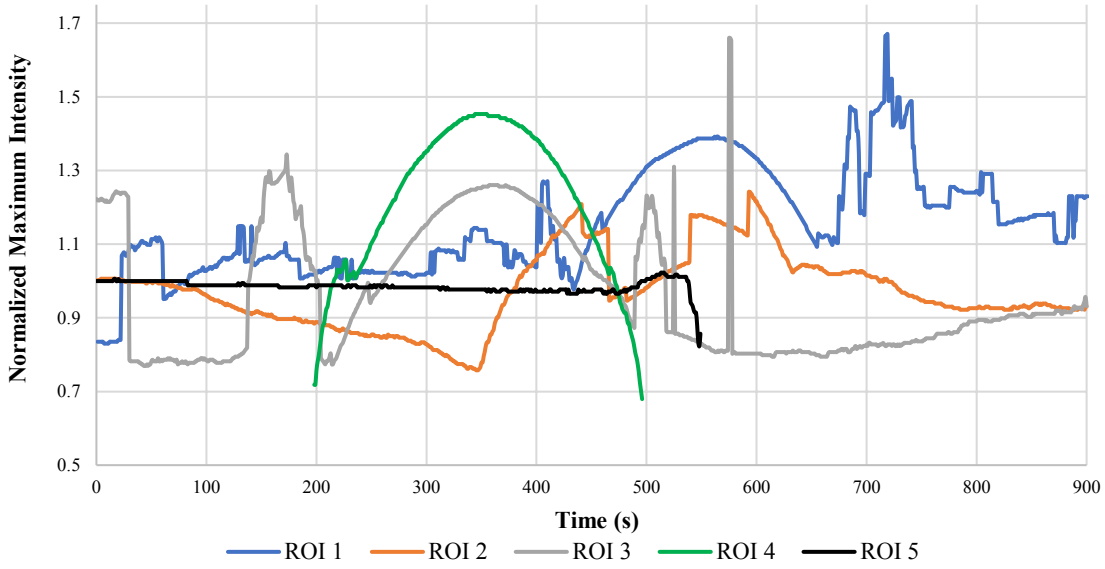

Figure 4. Normalized maximum signal intensity over time for 5 identified ROIs during a representative experiment of a 200 µM chloroquine addition at 300 s.

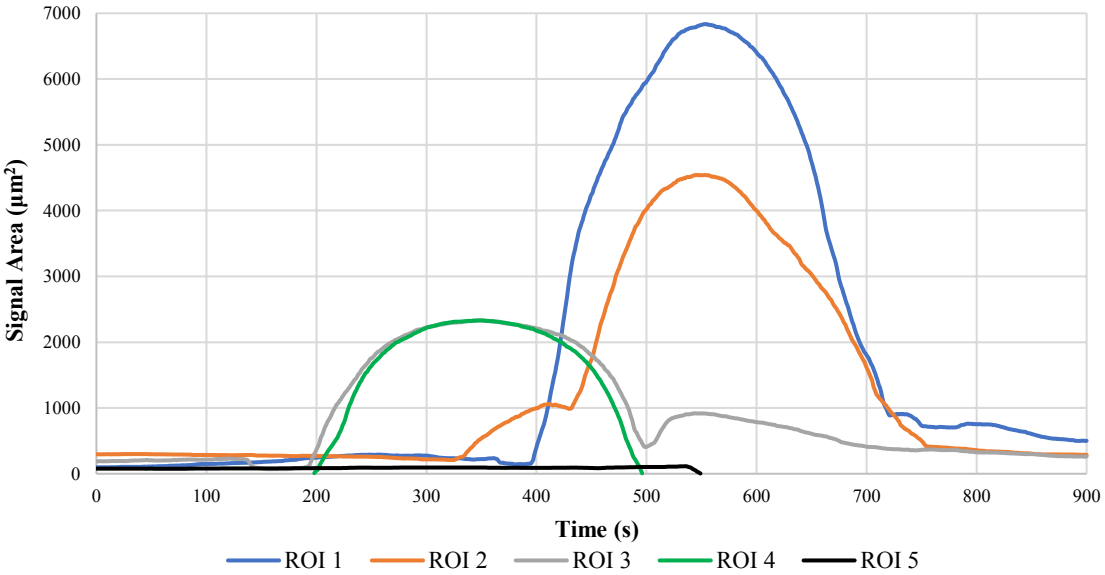

Figure 5. Signal area over time for 5 identified ROIs during a representative experiment of a 200 µM chloroquine addition at 300 s.

While S8 identified 381 ROIs in the field of view for the representative experiment shown in Figures 4 and 5, parameters for only five of these ROIs are plotted for representation purposes. Additionally, not all ROIs are above the set intensity threshold for the whole experiment time course of 900 s. For example, S8 no longer took measurements for ROI 4 shown in green past 500 s. Similarly, for ROI 5 shown in black, S8 stopped recording measurements past ~550 s. Furthermore, the first wave responses of normalized maximum intensities only lasted ~50 – 75 s after agonist addition then returned to or dropped below baseline values. Figures 4 and 5 were generated using the S8 output data and also provide information on the duration that each ROI of Ca^{++} signals was above the set threshold. For example, for ROIs 4 and 5, their average intensities dropped below the threshold around 500 s, so S8 stopped measuring their parameters such as maximum pixel intensity and signal area. By comparing all four parameter measurements at different agonist concentrations, S8 allowed for the identification of any concentration dependencies in the responses. ImageJ was used to apply an artificial color bar to both the raw and processed images to track the Ca^{++} signal maximum intensity and area over time for each ROI to illustrate how spatial and temporal differences in Ca^{++} gradients contribute to ASM constriction or relaxation (Figures 6 and 7). Figure 7 represents the pseudo-colored processed images outputted by S8 for a representative experiment. Using ImageJ, the outputted image masks were subsequently binarized to obtain black and white images illustrating the identified signal areas over time (Figure 8).

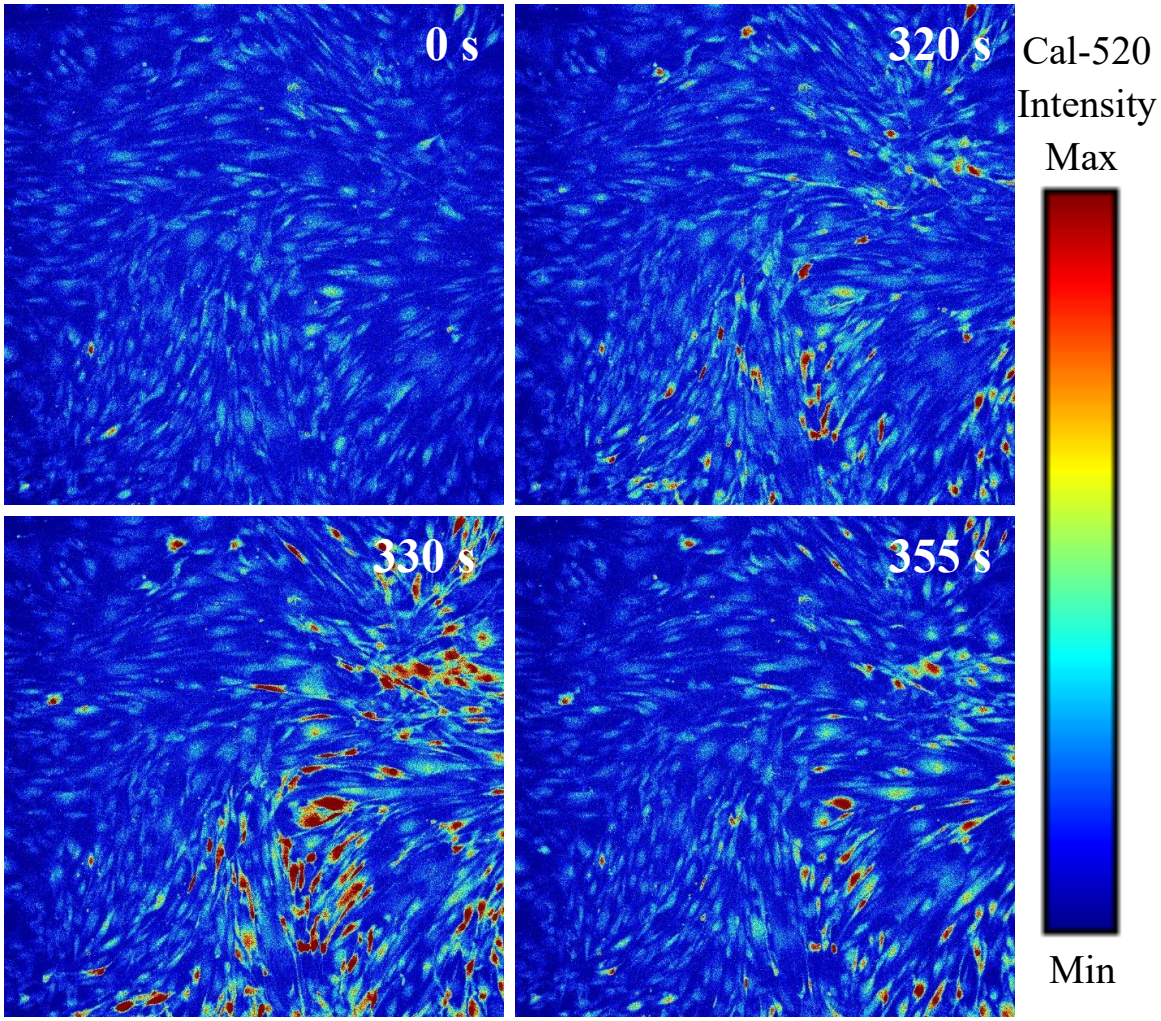

Figure 6. Pseudo-colored raw confocal images of the time course of saturating 200 µM chloroquine-induced Ca^{++} signals in HASMCs. The spatial patterns and intensities of chloroquine-induced (200 µM) Ca^{++} signals are shown at three time points (320 s, 330 s, and 355 s) following agonist addition at 300 s and compared to the baseline Ca^{++} activity at 0 s. Note that the signals appear to be nuclear in origin and propagate outwards to perinuclear regions of the cells. Signal intensity of the Cal-520® fluorophore is directly correlated to the concentration of Ca^{++} in HASMCs.

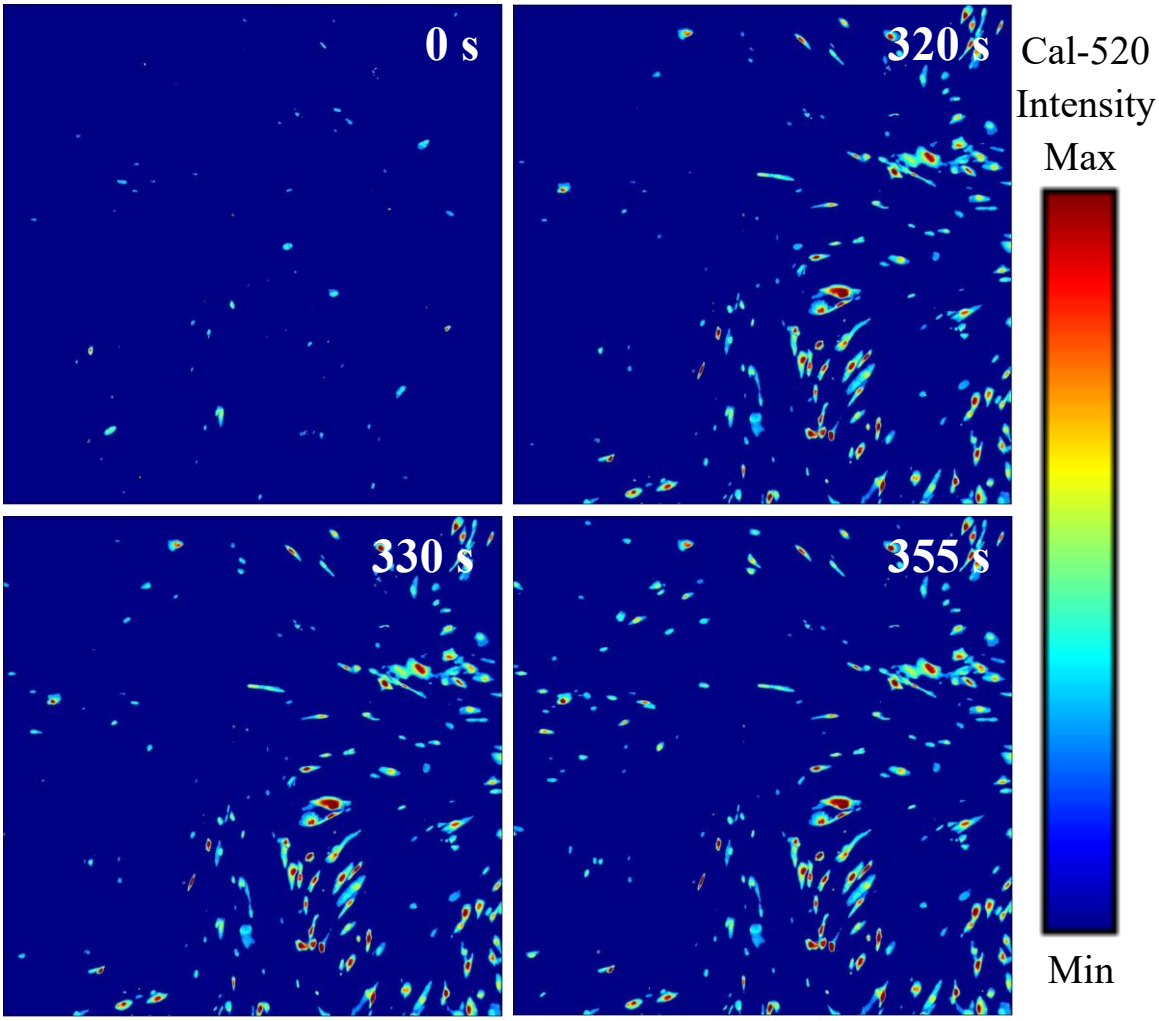

Figure 7 Pseudo-colored processed images of the time course of saturating 200 µM chloroquine-induced Ca^{++} signals in HASMCs. The spatial patterns and intensities of chloroquine-induced (200 µM) Ca^{++} signals are shown at three time points (320 s, 330 s, and 355 s) following agonist addition at 300 s and compared to the baseline Ca^{++} activity at 0 s. Note that the signals appear to be nuclear in origin and propagate outwards to perinuclear regions of the cells. Signal intensity of the Cal-520® fluorophore is directly correlated to the concentration of Ca^{++} in HASMCs.

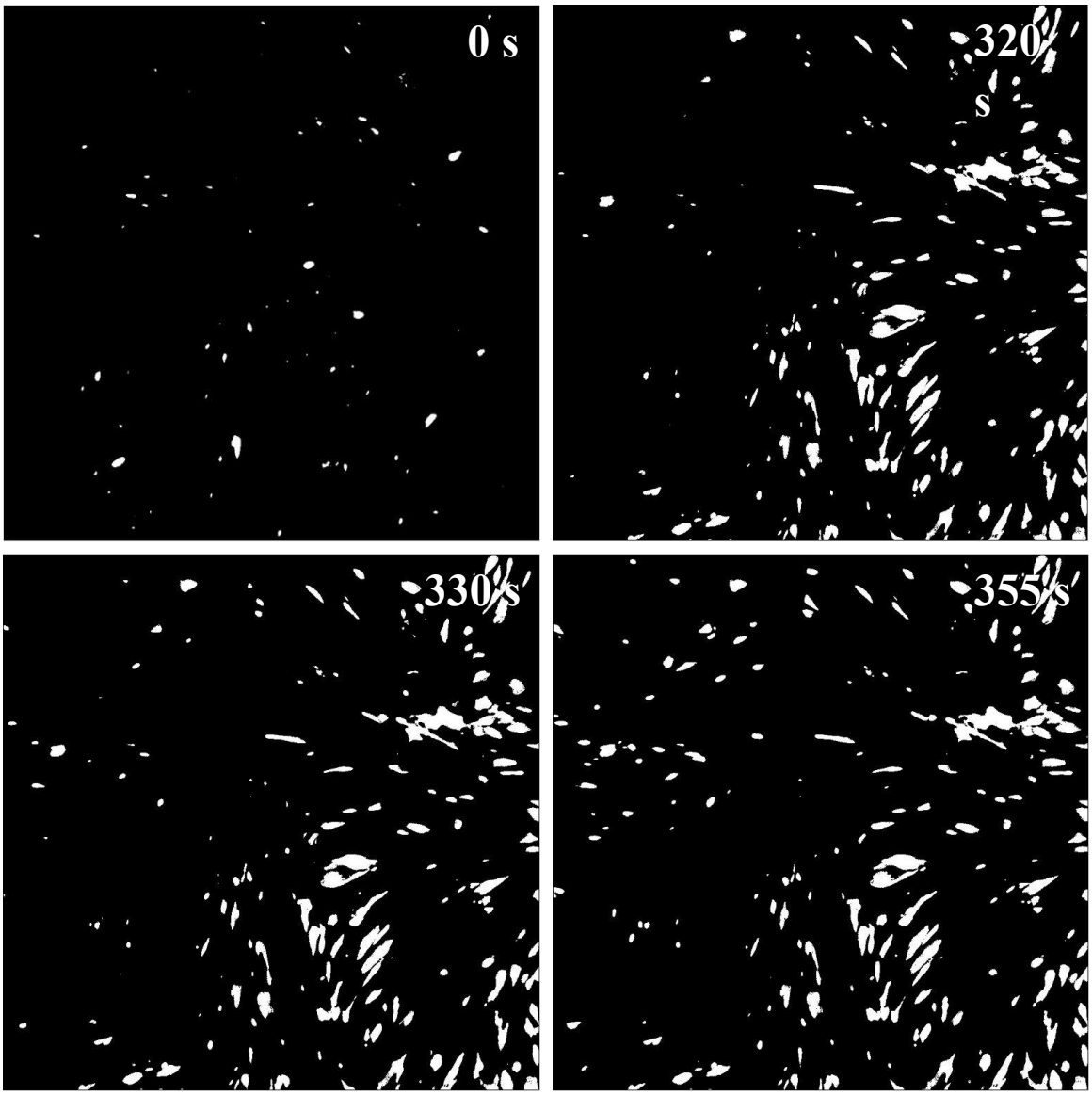

Figure 8. Black and white (binary) mask of processed images illustrating the signal area at four time points for all detected ROIs. The chloroquine-induced (200 μM) identified Ca^{++} signal areas are shown at three time points (320 s, 330 s, and 355 s) following agonist addition at 300 s and compared to the baseline Ca^{++} areas detected at 0 s.

CHAPTER VI: RESULTS AND DISCUSSION

6.1 Carbachol-Induced Ca^{++} Signals

The spatial propagation and intensity gradients of Ca^{++} signals induced by a saturating concentration (50 μM) of carbachol, a contractile G_q agonist, are shown at three time points (315 s, 322 s, and 360 s) following agonist addition at 300 s and compared to the baseline Ca^{++} activity at 0 s for a representative experiment in Figure 9.

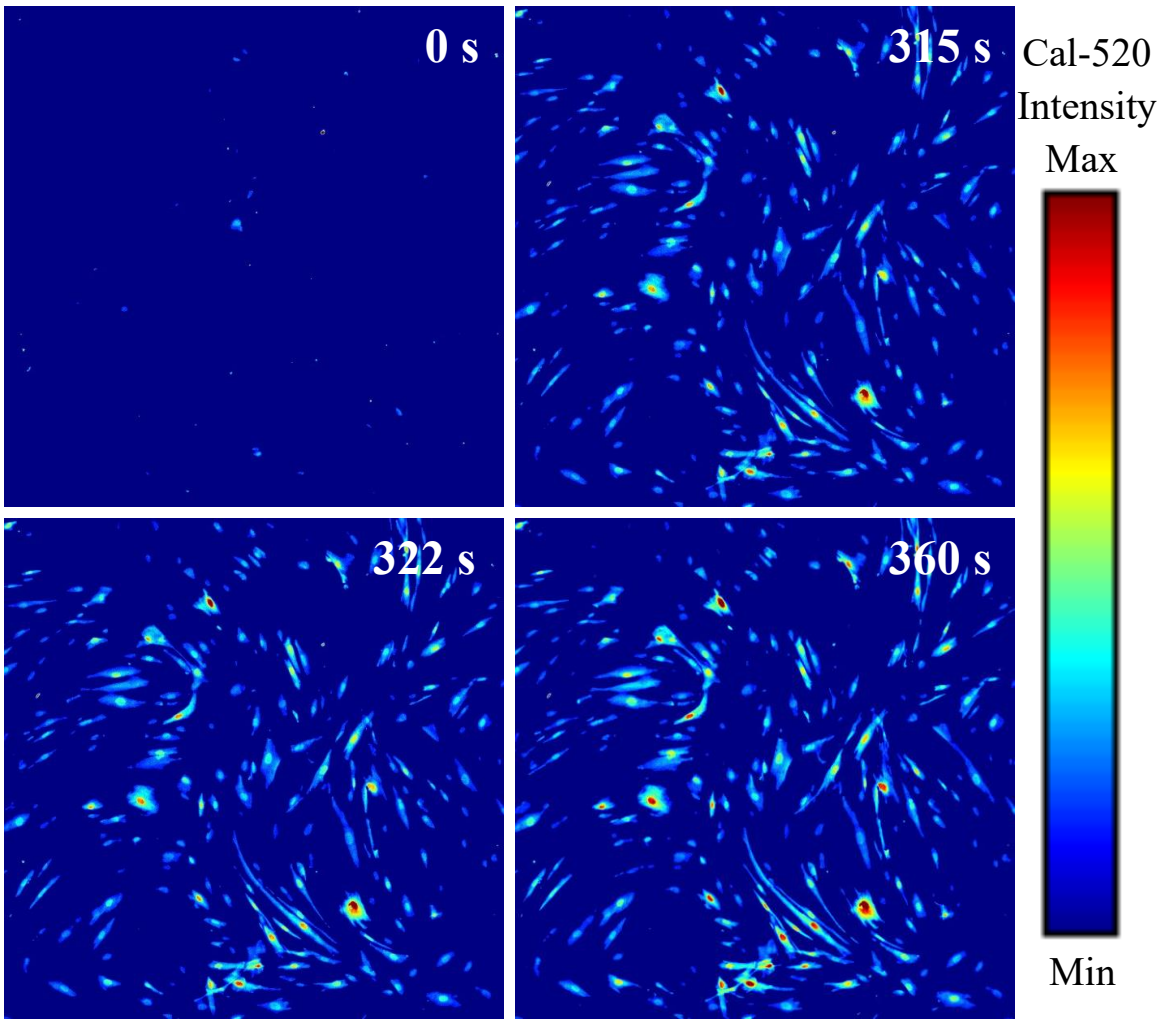

Figure 9. Pseudo-colored processed images of the time course of saturating 50 µM carbachol-induced Ca^{++} signals in HASMCs.

At the first time point, the basal Ca^{++} activity was low. Therefore, S8 did not detect many regions in the first frame as depicted in these processed images. Shortly after the agonist addition, many ROIs had an average intensity over the set threshold, which is apparent in the image at 315 s when compared to the baseline image at the beginning of the experiment. These processed images show both the area of each distinct Ca^{++} signal ROI for the given time points and the intensity gradient within each ROI over time.

These temporal and spatial propagations of Ca^{++} signals are illustrated through the intensity color gradient. The above Ca^{++} signal responses at the four time points represented were characterized by propagating waves, and the normalized maximum intensity versus time course graph, analogous to the one presented in Figure 4, may show subsequent Ca^{++} signal waves. Additionally, as seen in the image frames at 315 s, 322 s, and 360 s, some detected cells or ROIs overlap and cannot be detected separately by S8.

The images presented in Figure 9 for a saturating concentration of carbachol can be compared to the responses seen in Figure 10 when HASMCs are treated with the vehicle control (DMSO in a modified Tyrodes buffer) for carbachol. In this experiment, the vehicle control was added at 300 s following the procedure for all the experiments performed for this project. Minimal baseline Ca^{++} activity at the beginning of the experiment was detected. 15 s after the vehicle control addition, S8 detected more regions with average intensities above the set threshold, but there are markedly fewer identified regions than for a saturating concentration of carbachol. The detected signal areas appear to be much smaller than the regions detected in Figure 9. Near the end of the first wave response at 360 s, many ROIs that were previously detected had an average pixel intensity below the threshold, so S8 stopped measuring them, as indicated by their disappearance in the frame at 360 s.

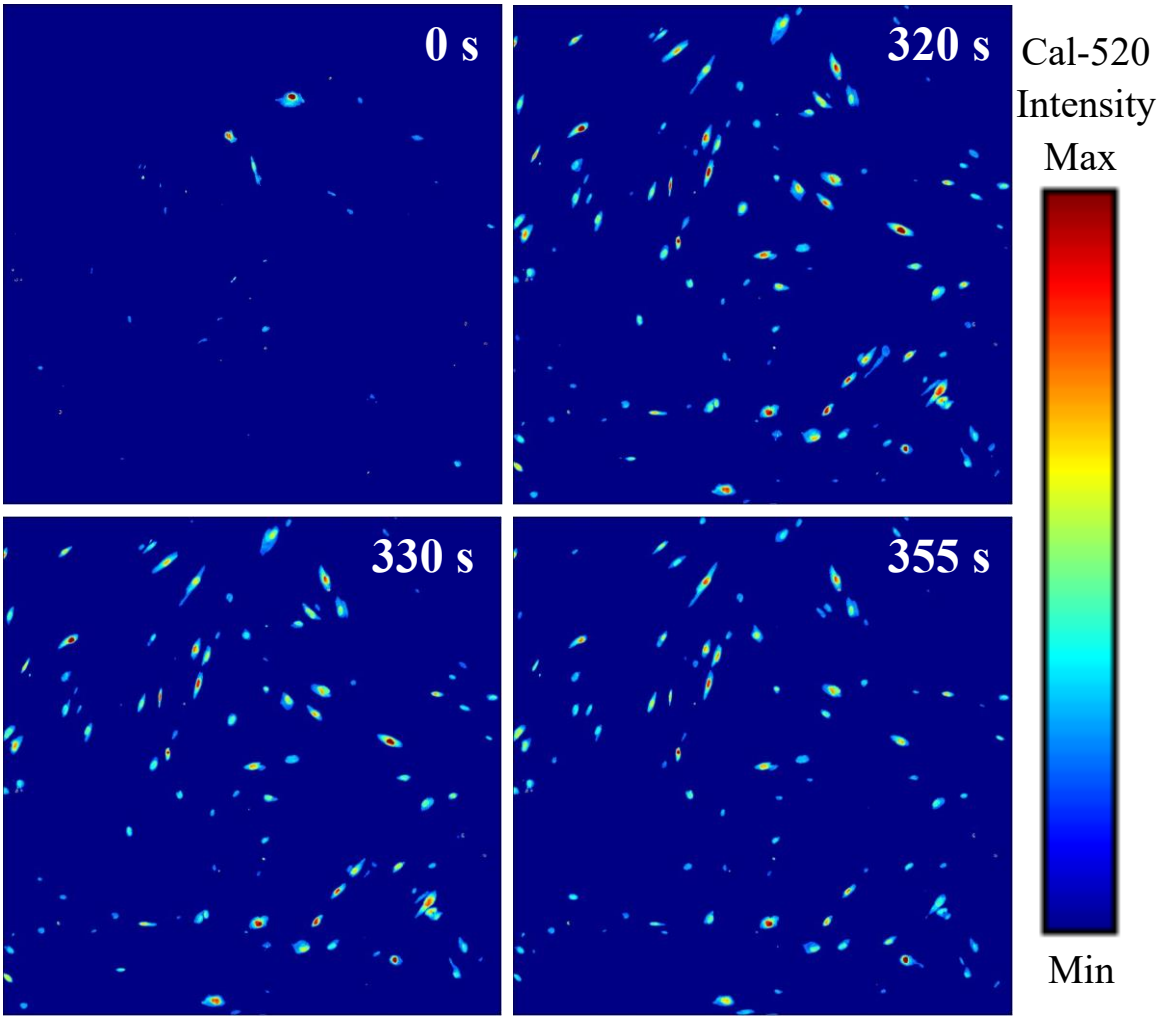

Figure 10. Pseudo-colored processed images of the time course of 0 µM carbachol (DMSO vehicle control)-induced Ca^{++} signals in HASMCs.

Results for some concentrations were only obtained from one experiment. The trends discussed for the following results are coupled with the recognition that additional experiments are required to determine whether results are statistically significant. The plot in Figure 11 panel *A* is a concentration-response curve showing the normalized average maximum intensity of all the identified ROIs for each concentration of carbachol tested. The "n" within each bar indicates the number of experiments performed for a given

concentration. However, before the trends and interpretations from these plots can be discussed, the S8 output data must be understood.

S8 identifies distinct regions of interest based on groups of pixels that are above the intensity threshold it sets. S8 can record the maximum pixel intensity within each identified ROI at every time point that the ROI is detected. The normalized values shown in Figure 11 panel *A* represent the ratio of the average maximum response intensity for all identified ROIs from 300 s until the end of the experiment in response to a given concentration of carbachol, to the average maximum baseline intensity from 0 to 60 s for all identified ROIs.

Lastly, for all concentrations with "n's" greater than 1, averaging all maximum "baseline" and "response" intensities allowed the calculation of the normalized average maximum intensity for all experiments of a given concentration.

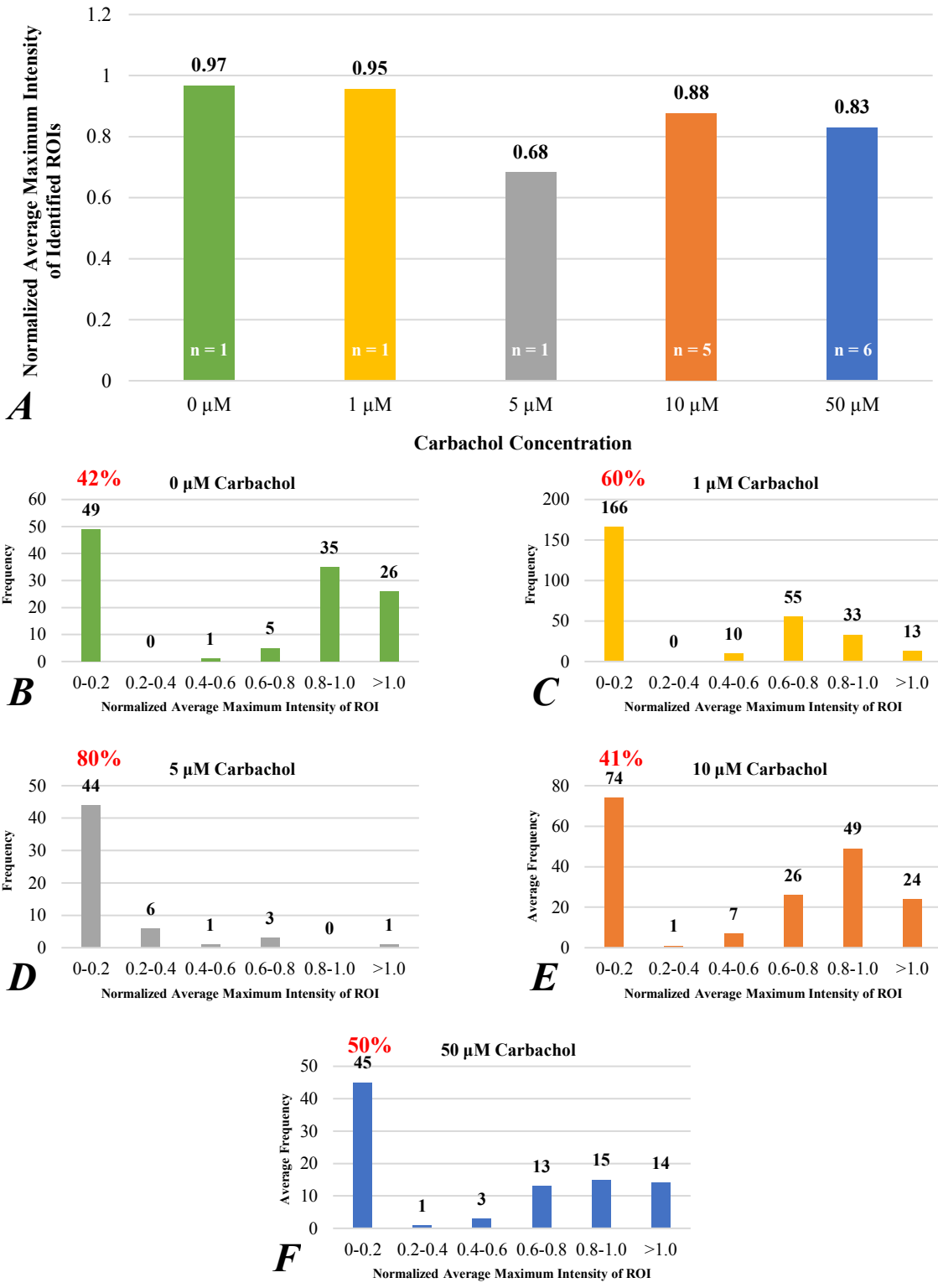

Figure 11. ***A*****, Normalized average maximum intensity concentration-response curve generated from outputted S8 measurements for carbachol.** ***B-F*****, Frequency distributions for carbachol.**

The distributions in Figure 11 panels *B-F* indicate the range of normalized maximum pixel intensities, which were averaged to obtain the normalized average maximum intensity concentration-response curve displayed in panel *A*.

The values presented in Figure 11 panels *A-F* were normalized to correct for any potential differences in the Cal-520® AM loading conditions, which could result in artificially high or low average maximum intensities. Normalizing the responses also corrected for any baseline Ca^{++} firing occurring before the agonist was added. The normalized values indicate the fold change (F/F_0) in average maximum intensity from the baseline due to the agonist addition. As seen previously in Figure 4 depicting the normalized peak intensity graph over time for 5 representative ROIs, the peak wave responses lasted ~50 – 75 s. Importantly, with the analysis method used to generate the figures in this section, an average from the time of addition at 300 s to the end of the experiment at 900 s was taken to capture all of the Ca^{++} wave responses. However, lower peak intensity values due to factors such as receptor desensitization at later time points could drive this average down, which explains why the values are close to 1.

At lower concentrations such as 0 μM and 1 μM, there was a ~5% decrease in the average maximum intensity from the baseline. As seen in Figure 10 presenting the processed images at four time points for a DMSO vehicle control addition, the cells did indeed respond after the addition, although it was a control experiment. Because this value is representative of one experiment, this increase in intracellular Ca^{++} concentration can either be due to a particular cover slip having highly active VDCCs, or the vehicle addition was made too forcefully causing the cells to stretch, activating their Ca^{++} channels, and leading to depolarization and contraction. With higher concentrations of carbachol (10 and

50 μM), there was a ~10% and 17% percent decrease in the normalized average maximum intensity from the baseline, respectively. However, for both 10 μM and 50 μM, two of the experiments were possible outliers that shifted these normalized values, which could be confirmed with future experiments. Treatment with 5 μM carbachol resulted in a 32% fold-change decrease in the normalized average maximum intensity from the baseline. Similarly, this data was obtained from one experiment, but may indicate that 5 μM carbachol is an outlier in the aforementioned trends.

To further explore these trends, a distribution of the normalized average maximum intensities was created for each concentration tested. For concentrations whose normalized values were obtained from multiple experiments, the frequency of each bin was averaged to obtain the presented values. These distributions indicate that ~50% of the normalized average maximum intensities for each concentration were between 0 and 0.2, meaning that the response is not multimodal. This also suggests that the response seen after treatment with 5 μM carbachol may be an outlier, because it does not follow this trend. Instead, ~80% of the recorded Ca^{++} responses exhibited a normalized maximum average intensity between 0 and 0.2.

Similar to the methods used in generating the carbachol ROI normalized maximum intensity plot shown in Figure 11 panel *A*, the carbachol average ROI area concentration-response curve was generated by averaging the Ca^{++} signal area from 300 to 900 s for all identified ROIs and is presented in Figure 12 panel *A*. For reference, an HASMC is ~250 μm in length and 3 – 5 μm in width on average at the z-level of the nucleus.[25] While these larger area values presented in Figure 11 panel *A* could suggest significant increases in Ca^{++} signal area throughout an entire cell, it is likely that the S8 software could not

consistently distinguish between two or more cells or ROIs overlapping, as indicated earlier in Figure 10.

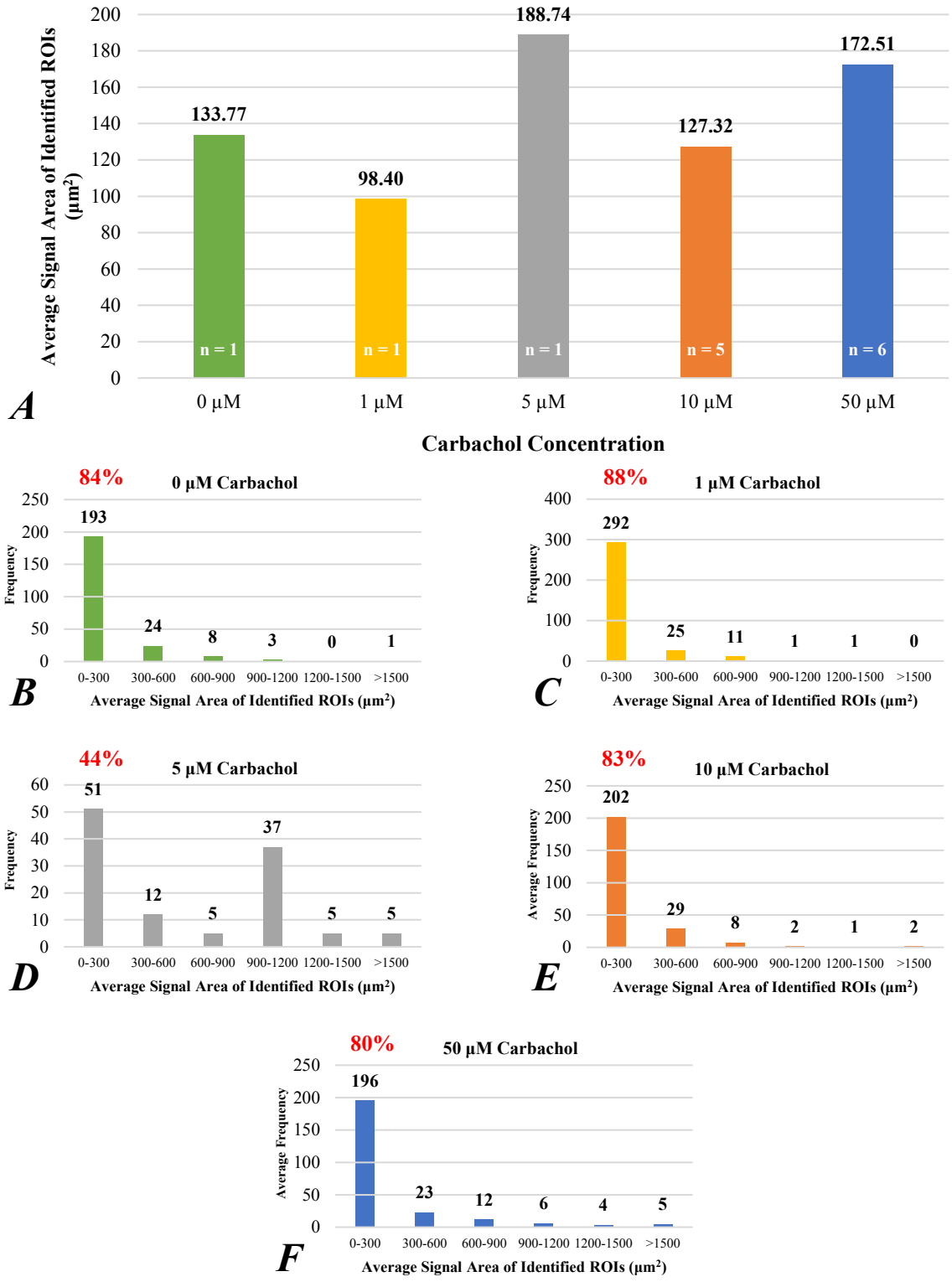

Figure 12. ***A*****, Identified average signal area concentration-response curve generated from outputted S8 measurements for carbachol.** ***B-F*****, Frequency distributions for carbachol.**

The average signal area values thus confirm what was depicted in the processed images presented in Figure 10. For a saturating concentration of carbachol, the average signal area detected by S8 was 173 μm^2, or ~30% larger than the baseline Ca^{++} responses in the control experiment and ~75% larger than the responses seen at 1 μM. The concentration-response curve for average Ca^{++} signal areas further confirms that the values obtained from treatment with 5 μM may be outliers. Additionally, receptor desensitization may occur at higher concentrations leading to the ~10% greater average Ca^{++} response area seen at 5 μM compared to 50 μM. The frequency distributions depicted in panels *B-F* further indicate that 5 μM carbachol may be an outlier. While the average signal area after agonist addition was ~30% larger for 50 μM than for the control, more experiments need to be performed to determine if this trend holds true. Otherwise, these frequency distributions illustrate that for all concentrations except 5 μM, ~85% of all the detected signal areas for each concentration were smaller than 300 μm^2, suggesting no concentration dependence on Ca^{++} signal area in response to carbachol.

The third parameter studied was the duration of the carbachol responses after the agonist addition at 300 s. While a ~30% increase in average signal area from 0 to 50 μM is illustrated in Figure 12 panel *A*, the average signal duration concentration-response curve in Figure 13 panel *A* indicates a ~72% increase in average signal duration from the control to the saturating concentration. For a given concentration, the numbers shown represent the average duration of all ROIs after the agonist addition was made at 300 s. For concentrations with an "n" > 1, an average of averages was taken. The two characteristic peaks exhibited in Figure 13 panel *E* show that the majority (~78%) of the responses to 10 μM carbachol are either transient (between 0 and 40 s) or propagating waves lasting longer

than 200 s. The same trend is seen for a saturating concentration, where ~56% of the responses are either transient or prolonged. At lower concentrations, such as 0 μM and 1 μM, the majority of the responses are transient (less than 40 s), again demonstrating that the experiment performed for 5 μM carbachol may be an outlier. Excluding this experiment, a general trend is apparent such that higher concentrations of carbachol (e.g. 10 μM and 50 μM) elicit an increase in Ca^{++} signals longer than 200 s and a loss of transient signals.

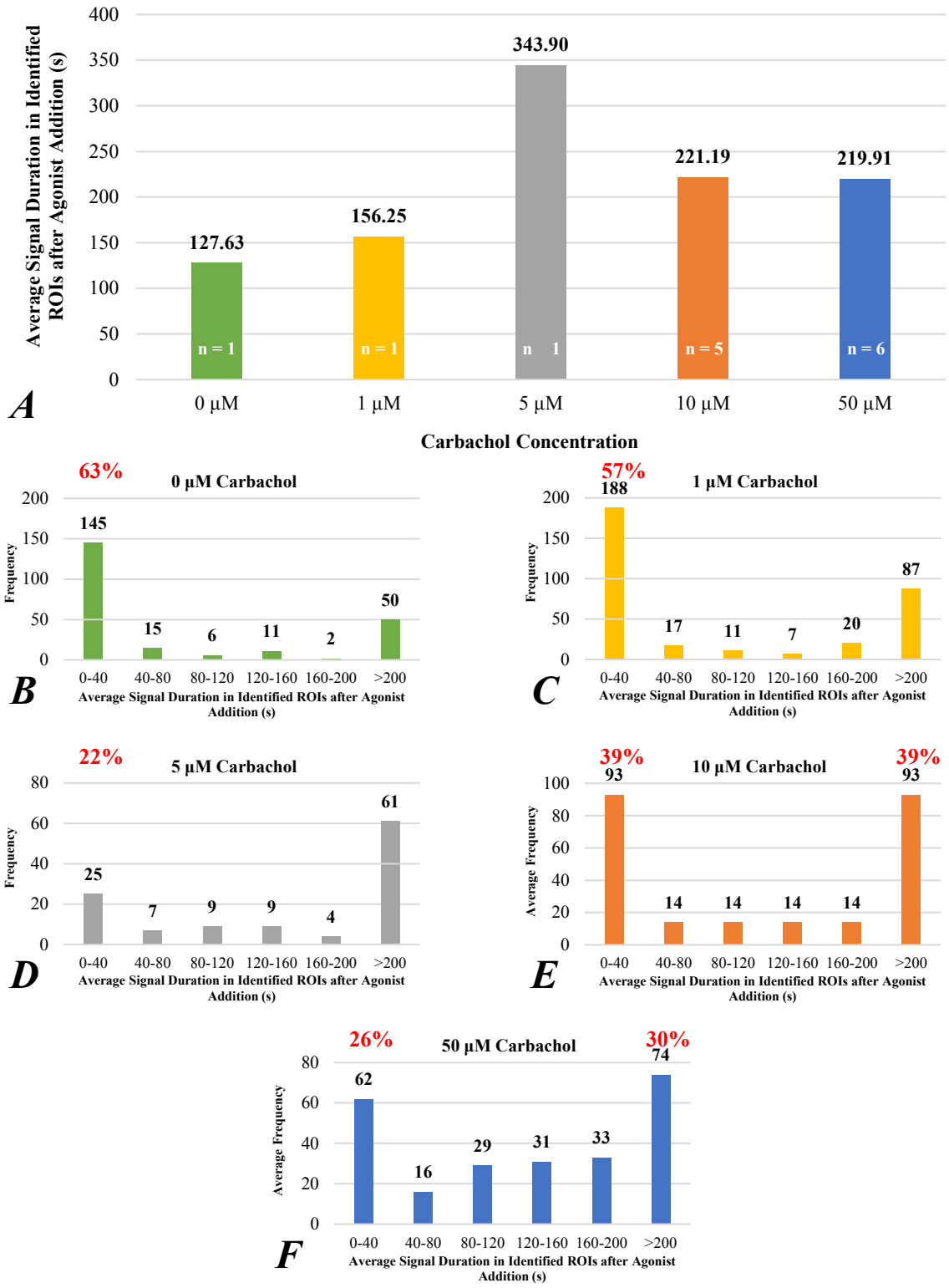

Figure 13. ***A*****, Average signal duration concentration-response curve generated from outputted S8 measurements for carbachol.** ***B-F*****, Frequency distributions for carbachol.**

The fourth parameter studied was the number of Ca^{++} responses detected. Figure 14 illustrates that treatment with 1 μM carbachol resulted in a ~44% average increase in the number of responses compared to the control experiment. However, as seen in Figure 13 panel *C*, over 50% of the responses to 1 μM carbachol were less than 40 s. At a low concentration of agonist addition such as 1 μM, the large number of shorter Ca^{++} responses to 1 μM carbachol may represent transient firings previously introduced as Ca^{++} "flashes." Additionally, the larger number of Ca^{++} signals detected at 1 μM could indicate Ca^{++} sparklets, which is supported by the average ROI signal area of 98.40 μm^2 as shown in Figure 12 panel *A*. Additionally, ~88% of the average ROI areas measured were smaller than 300 μm^2 after treatment with 1 μM carbachol. Conversely, the lower number of responses at higher concentrations such as 50 μM could be representative of receptor desensitization.

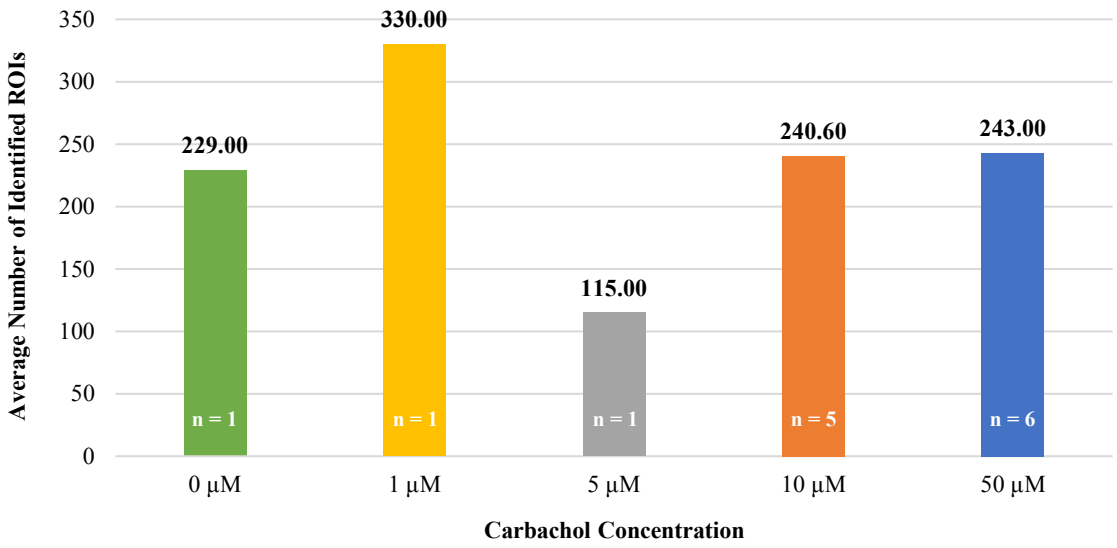

Figure 14. Average number of identified ROIs concentration-response curve generated from outputted S8 measurements for carbachol.

6.2 Chloroquine-Induced Ca^{++} Signals

The spatial propagation and intensity gradients of Ca^{++} signals induced by a saturating concentration (200 μM) of chloroquine, a bitter taste receptor G_q agonist that induces ASM relaxation, are shown at three time points (320 s, 330 s, and 355 s) following agonist addition at 300 s and compared to the baseline Ca^{++} activity at 0 s (Figure 15).

The images shown in Figure 15 can be compared to the responses seen in Figure 16 when HASMCs are treated with vehicle control, which for chloroquine, is water (H_2O) in a modified Tyrodes buffer. The time points chosen for these images are the same time points presented for chloroquine in Figure 15 so that the responses can be accurately compared.

In the representative vehicle control experiment presented in Figure 16, H_2O in a modified Tyrodes buffer was added at 300 s. However, unlike with the DMSO control experiment presented in Figure 10, this control experiment exhibited significant Ca^{++} activity after the addition was made. Even for this control experiment, S8 detected 223 regions with average intensities above the set threshold. Although this is fewer detected regions compared to the experiment presented in Figure 15 wherein 381 ROIs were detected in response to a saturating concentration of chloroquine, there are a few possibilities for this amplified response. Firstly, because one experiment was performed, further experiments may show markedly different responses. Moreover, this monolayer of HASMCs may have exhibited high baseline Ca^{++} activity, as illustrated in the baseline image at 0 s included in Figure 16. Although Figure 16 presents the Ca^{++} responses at four timepoints, images at subsequent time points during baseline acquisition consistently depict high baseline Ca^{++} concentrations, where the red false color spans the entire area of

some ROIs before and after the vehicle control was added. Another possibility for this amplified baseline Ca^{++} response is that cells were hypersensitize or hyperresponsive to mechanical perturbations if the vehicle addition was made too forcefully, causing the cells to stretch, opening and activating their VDCCs, and leading to depolarization and contraction. This increase in Ca^{++} concentration could specifically be mediated by mechanosensitive receptors such as the transient receptor potential cation channel subfamily V member 4 (TRPV4), which is a Ca^{++}-permeable cation channel that has been implicated in stretch mechanotrasduction in multiple cell systems and is expressed in the adult lung.[26]

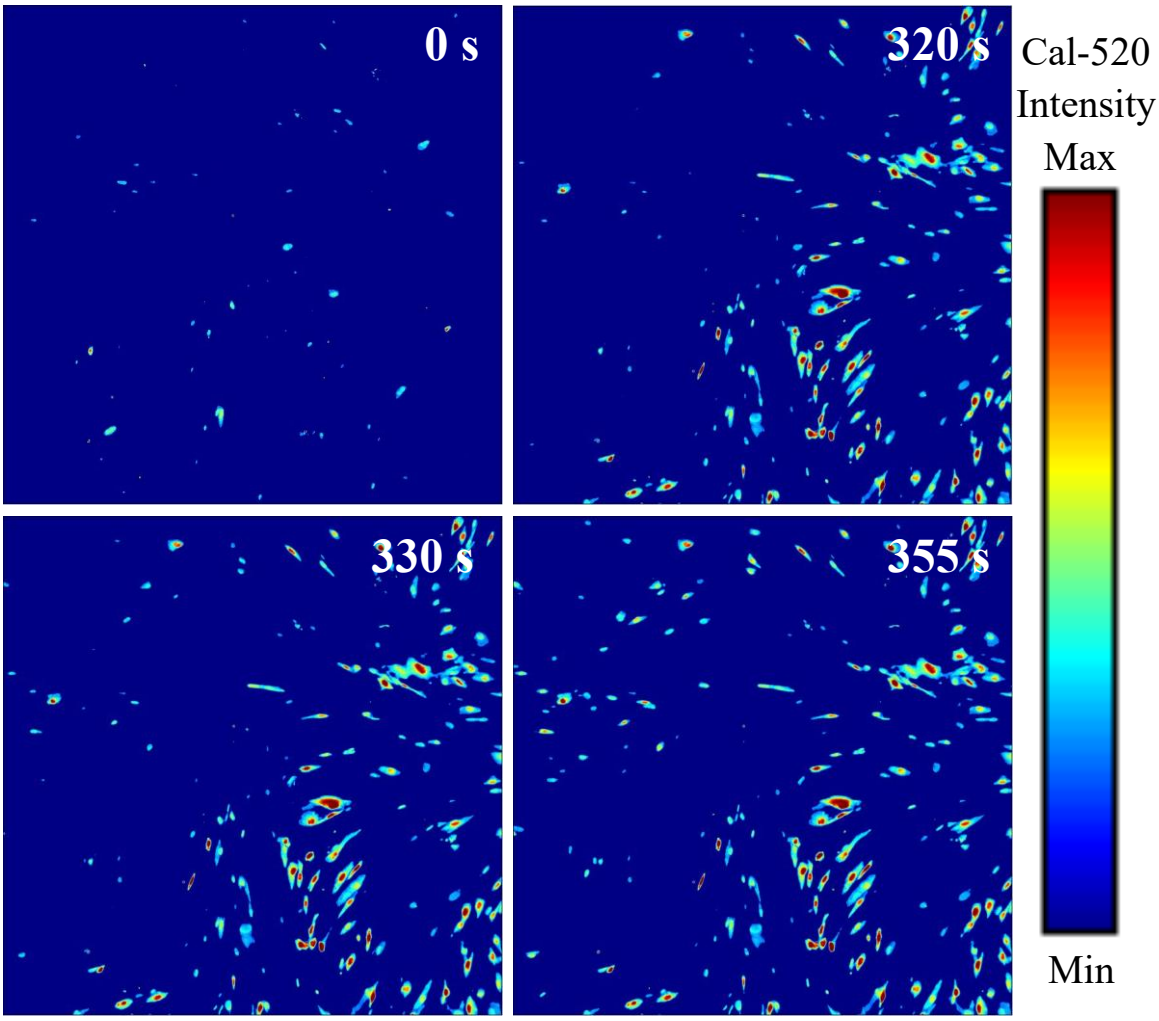

Figure 15. Pseudo-colored processed images of the time course of saturating 200 µM chloroquine-induced Ca^{++} signals in HASMCs.

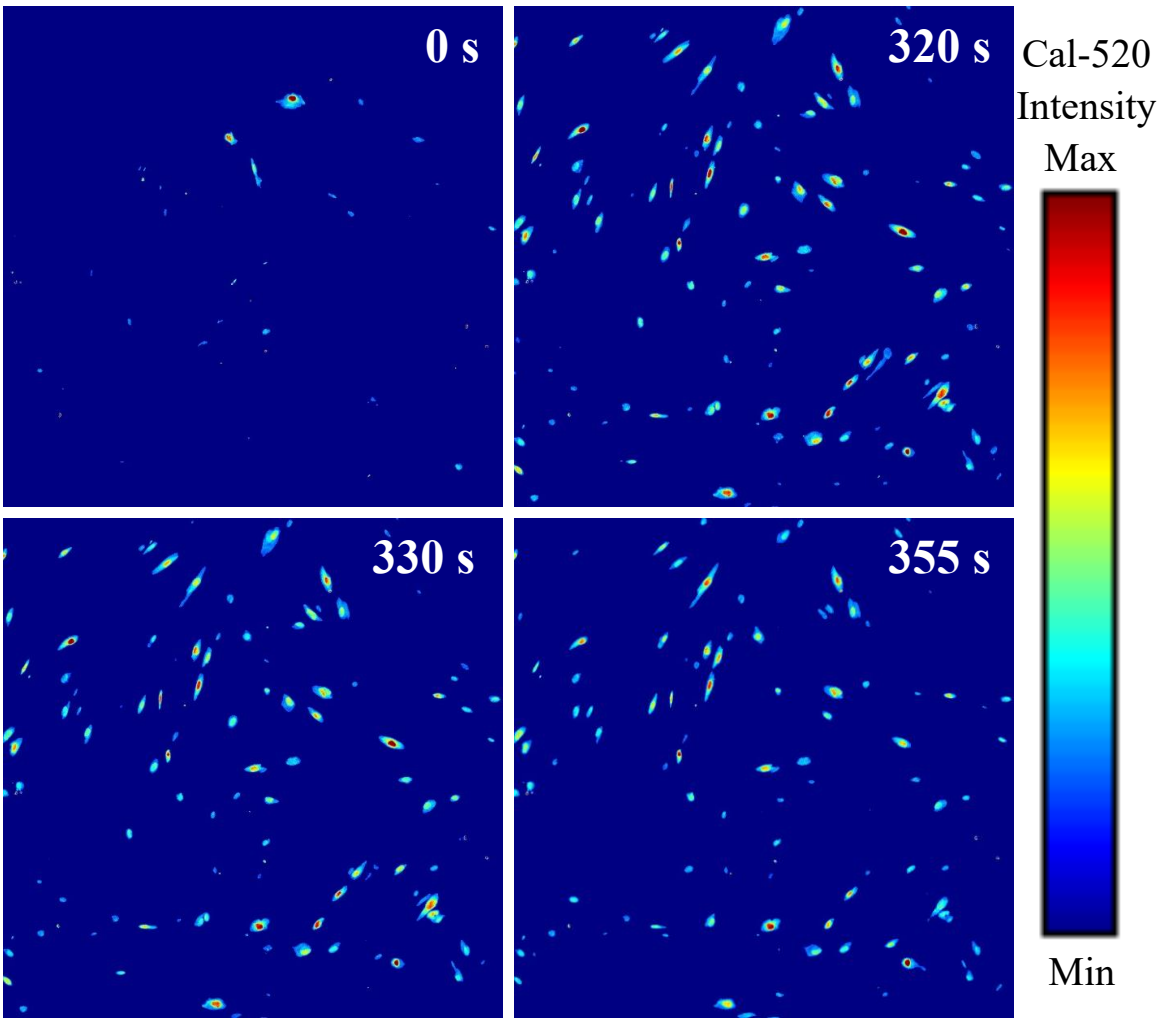

Figure 16. Pseudo-colored processed images of the time course of 0 µM chloroquine (H_2O vehicle control)-induced Ca^{++} signals in HASMCs.

The normalized peak intensity concentration-response curve for chloroquine was generated in the same manner as for carbachol and is depicted in Figure 17. Unlike carbachol, these data represent a bimodal response, where there is a ~10% decrease in the normalized average maximum intensity at 0 µM, 20 µM, 100 µM, and 200 µM, but a ~22% decrease at 10 µM, thus resulting in a curve with two groups of characteristic peaks. For

treatment with 20 μM chloroquine, both experiments exhibited similar average maximum baseline intensities of ~150 and average maximum response intensities of ~140.

A distribution of the normalized average maximum intensity was created for each concentration to determine if the plot in Figure 17 panel *A* could possibly be multimodal. These distributions indicate that ~60 – 70% of the normalized maximum intensities for all concentrations except 10 μM were between 0 and 0.2, whereas ~50% of the normalized maximum intensities were between 0 and 0.2 for 10 μM. This nonuniformity in response indicates that the normalized average maximum intensities for chloroquine may be concentration-dependent, although future supporting data is required.

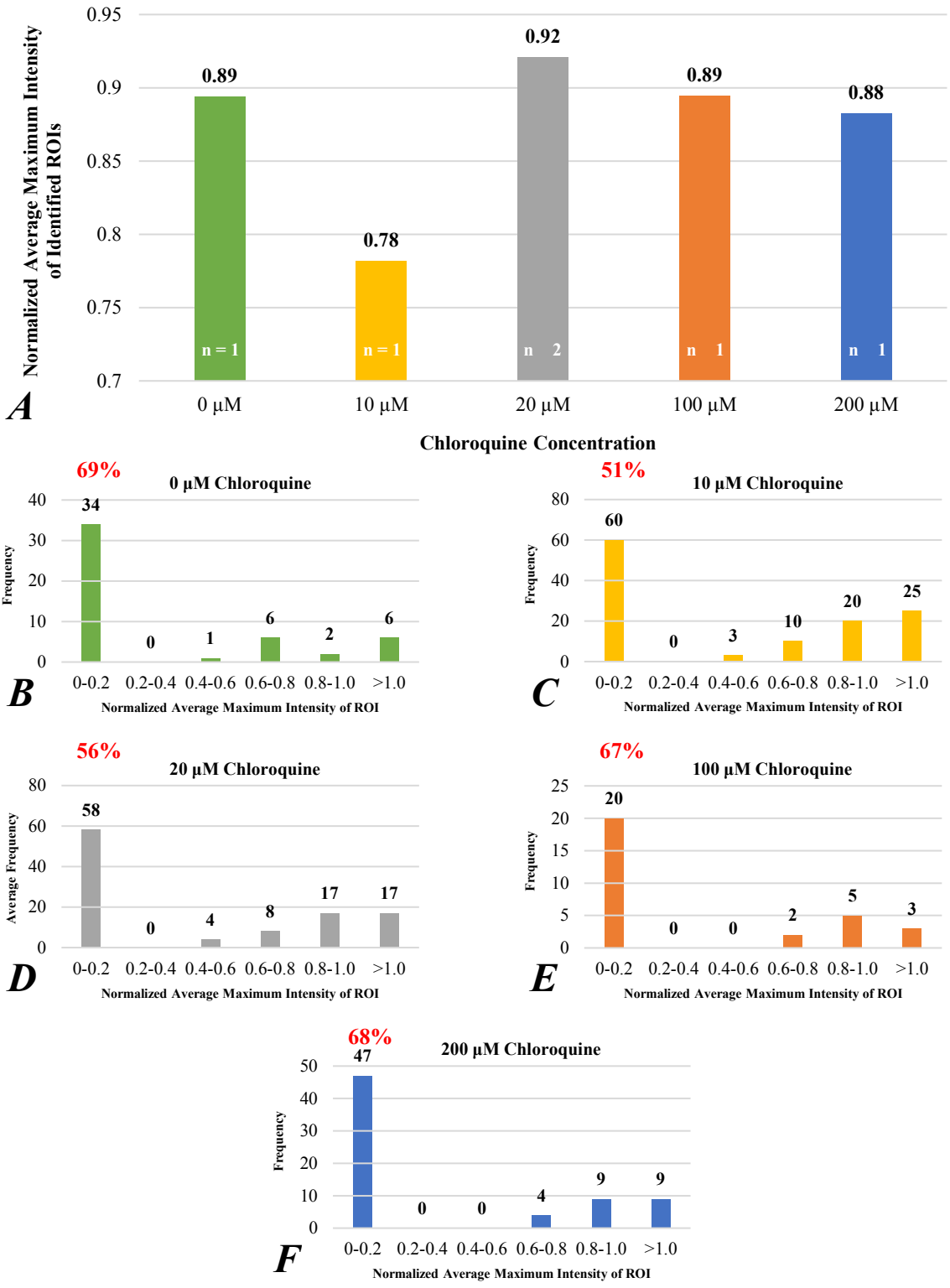

Figure 17. ***A*****, Normalized average maximum intensity concentration-response curve generated from outputted S8 measurements for chloroquine.** ***B-F*****, Frequency distributions for chloroquine.**

The concentration-response area curve for chloroquine was similarly generated using the same methods as for carbachol.

The average signal area values confirm what was indicated in the processed images presented in Figures 15 and 16, where the detected Ca^{++} signal areas for the control experiment were ~41% greater than for the saturating concentration. However, this could be due to the high baseline Ca^{++} activity as seen in Figure 16. Otherwise, the average Ca^{++} signal areas increased for increasing concentrations of chloroquine. Importantly, for 20 μM with an "n" of 2, the average signal areas were ~108 and 118 μm^2 for each respective experiment, indicating that neither experiment is a probable outlier.

Referencing the frequency distributions in Figure 18 panels *B*-*F* reflects this general trend for chloroquine-induced Ca^{++} signal areas as seen in the average signal area concentration-response curve in panel *A*. Likewise, excluding the control experiment, as the average signal area increases with increasing concentration, the percentage of Ca^{++} signal areas smaller than 300 μm^2 decreases.

Currently, fewer experiments have been collected for the G_q agonists chloroquine and histamine. Definitive trends cannot be speculated without warranting future experiments. Therefore, the concentration-response curves for both normalized average maximum signal intensity and average signal area will be presented and discussed in chapters 6.2 and 6.3. Both the ROI average signal duration and average number of identified ROIs concentration-response curves in response to chloroquine will be introduced in Appendix A, while the same plots albeit in response to histamine will be introduced in Appendix B.

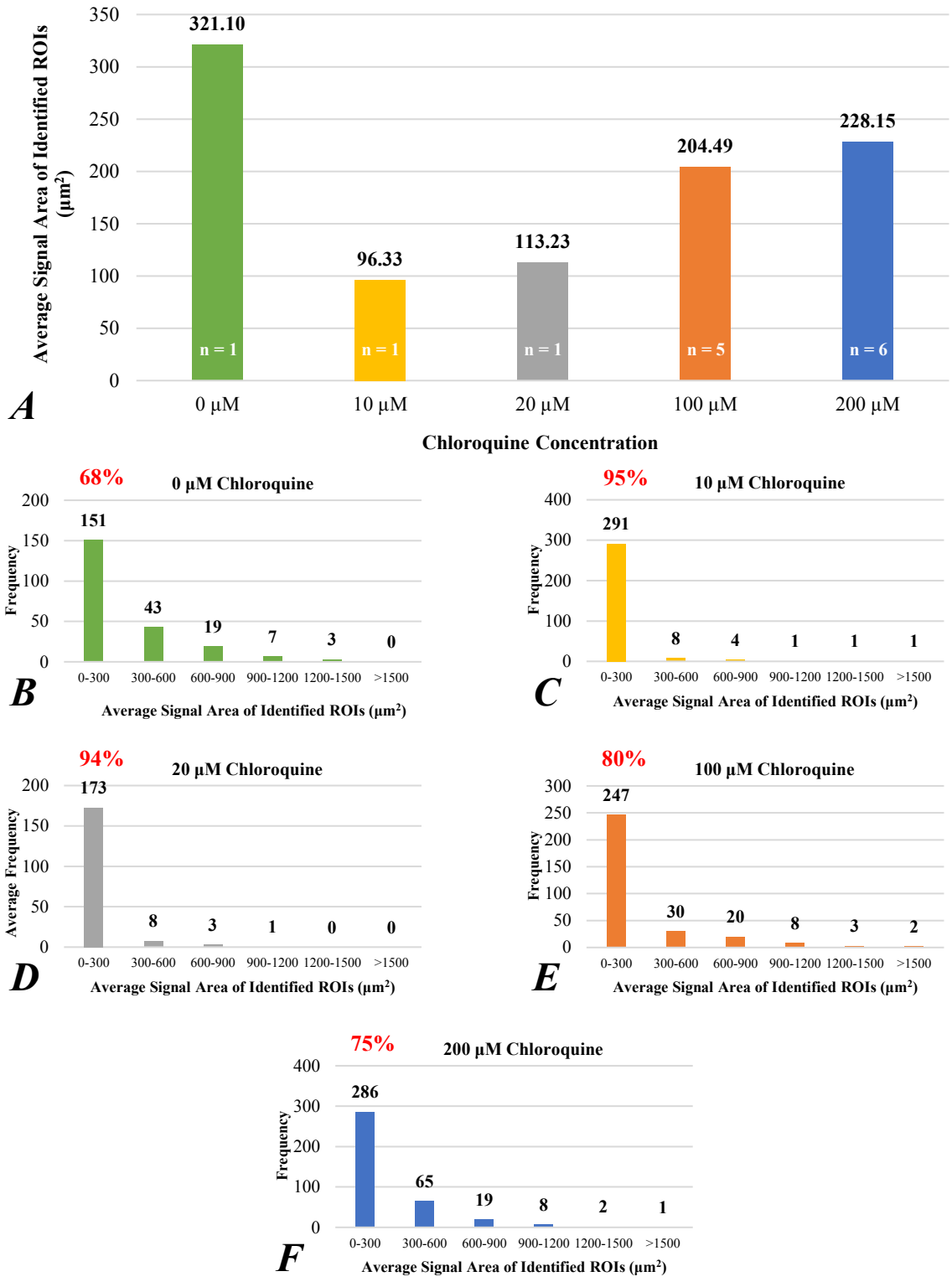

Figure 18. ***A*****, Identified average signal area concentration-response curve generated from outputted S8 measurements for chloroquine.** ***B-F*****, Frequency distributions for chloroquine.**

6.3 Histamine-Induced Ca^{++} Signals

The spatial propagation and intensity gradients of Ca^{++} signals induced by a non-saturating concentration (0.5 μM) of histamine, a contractile G_q agonist, are shown at three time points (400 s, 435 s, and 457 s) following agonist addition at 300 s and compared to the baseline Ca^{++} activity at 0 s for a representative experiment in Figure 19.

The images in Figure 19 can be compared to the responses seen in Figure 16 when HASMCs are treated with vehicle control, which for both histamine and chloroquine, is H_2O in a modified Tyrodes buffer.

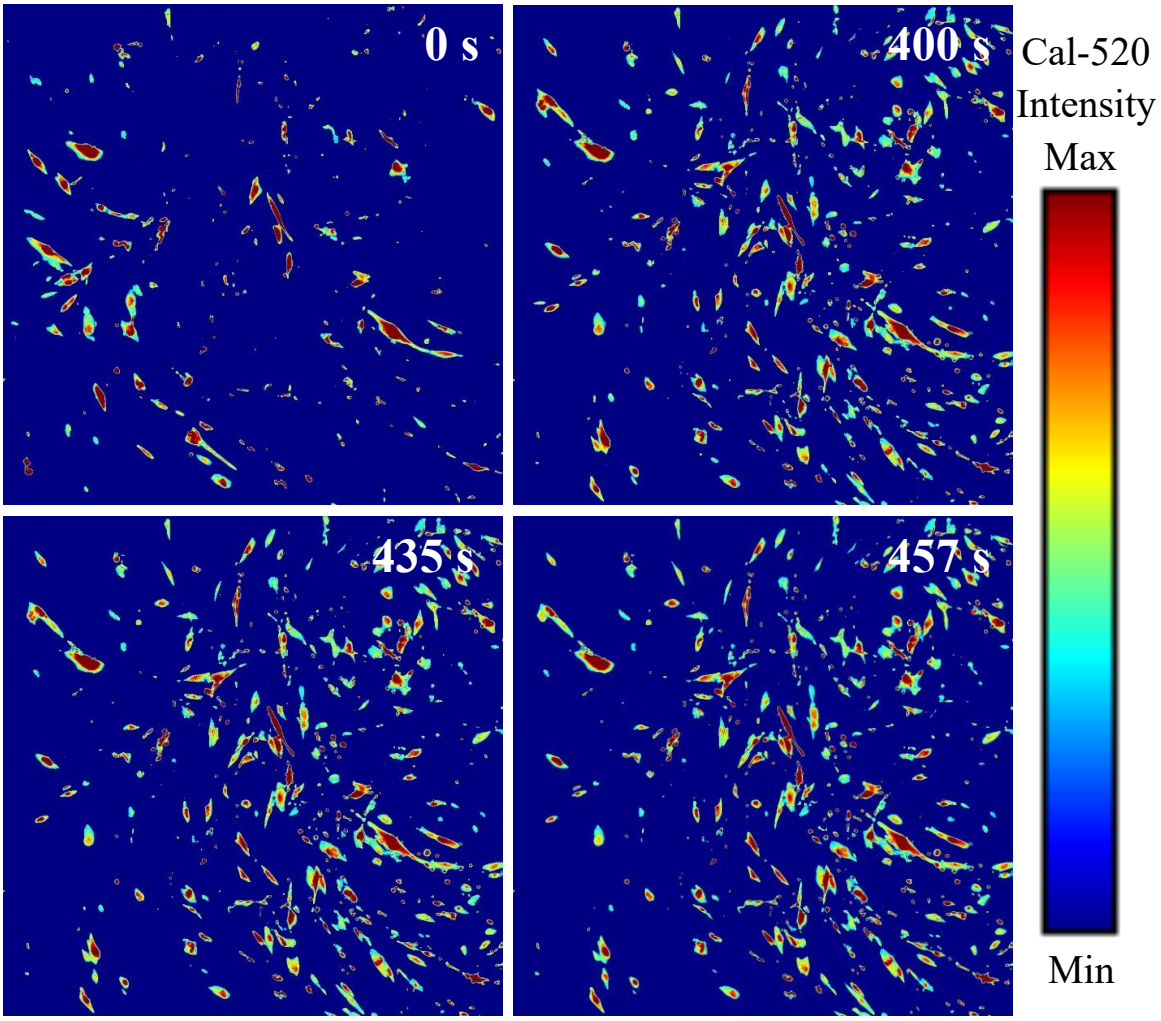

Figure 19. Pseudo-colored processed images of the time course of non-saturating 0.5 µM histamine-induced Ca^{++} signals in HASMCs.

The processed images shown in Figure 19 are for a representative experiment of the lowest concentration addition of histamine at 0.5 µM. At the start of the experiment, the baseline Ca^{++} activity was high as indicated by the red spreads indicating high Cal-520® fluorescence.

As seen in the processed image 100 seconds after the addition was made, although the baseline Ca^{++} activity was high, there were further increases in Ca^{++} activity after the

agonist addition, as more ROIs were detected. Over the course of this experiment, 506 ROIs had an average intensity above the set threshold.

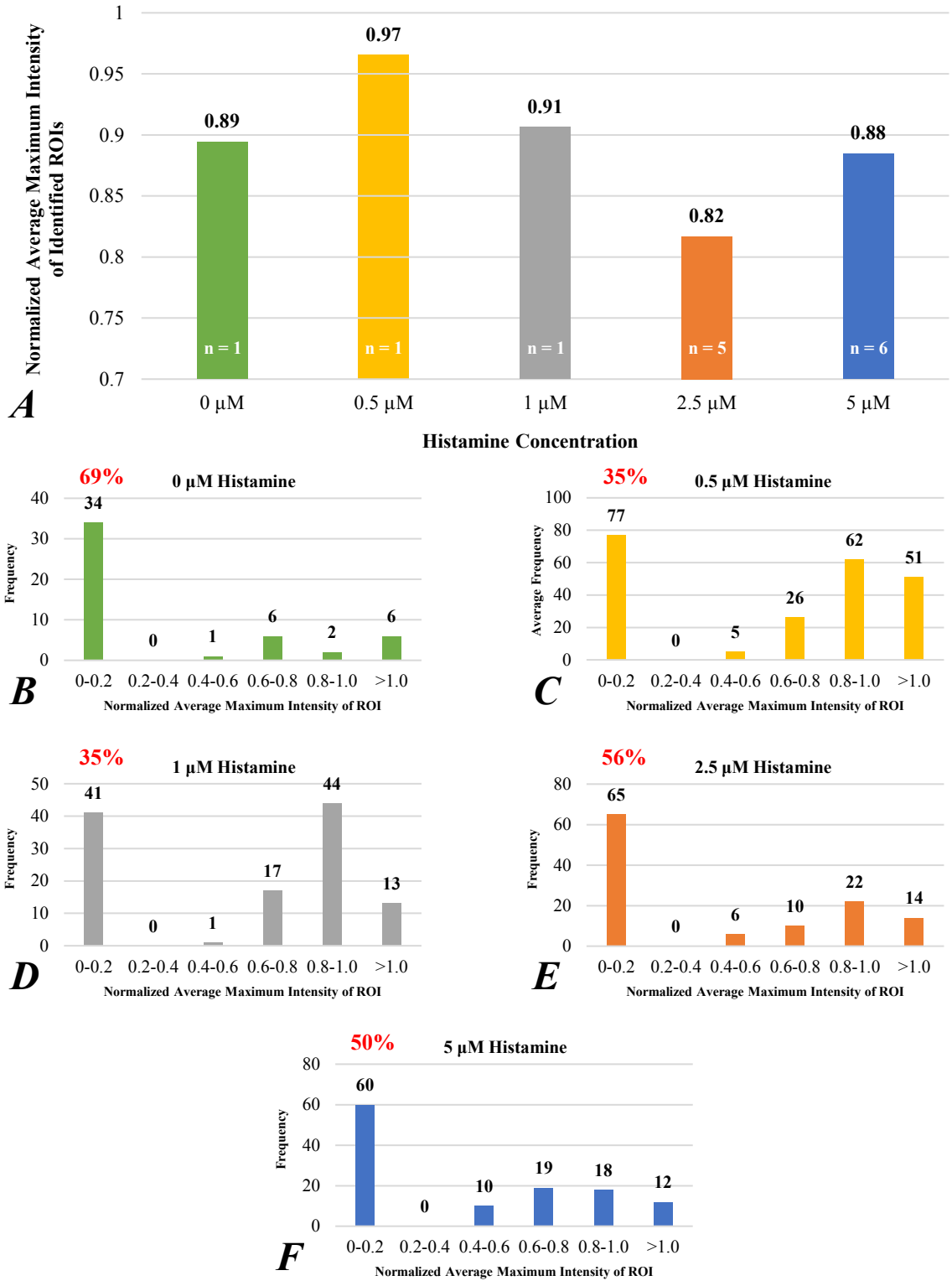

Figure 20. ***A*****, Normalized average maximum intensity concentration-response curve generated from outputted S8 measurements for histamine.** ***B-F*****, Frequency distributions for histamine.**

Figure 20 depicts the normalized peak intensity concentration-response curve that was generated in the same manner as for carbachol and chloroquine. In this case, there was no apparent increase or decrease in the normalized average peak intensity for the saturating concentration when compared to the control. While the Ca^{++} responses to 0.5 μM histamine may appear to be significant, it is important to note that this average value only represents an "n" of 2. Importantly, the average peak intensity is 330 arbitrary units (A.U.) for one experiment at 0.5 μM but only 60 A.U. for the other experiment at 0.5 μM. More data needs to be collected at this concentration to confirm that the measured responses are replicable.

A distribution of the normalized average maximum intensities was created for each concentration of histamine addition. Although there was no apparent increase or decrease in the normalized average peak intensity for the saturating concentration when compared to the control as seen in Figure 20 panel *A*, these distributions indicate that ~50% of the normalized peak intensities for higher concentrations were between 0 and 0.2, whereas ~69% of the normalized peak intensities for the control experiment were between 0 and 0.2. Furthermore, ~35% of the normalized peak intensity values were between 0 and 0.2 at lower concentrations. This suggests that the changes in peak Ca^{++} signal intensities induced by histamine are in fact concentration-dependent.

Figure 21 presents the concentration-response average signal area curve for histamine, which was generated using the same methods as for carbachol and chloroquine.

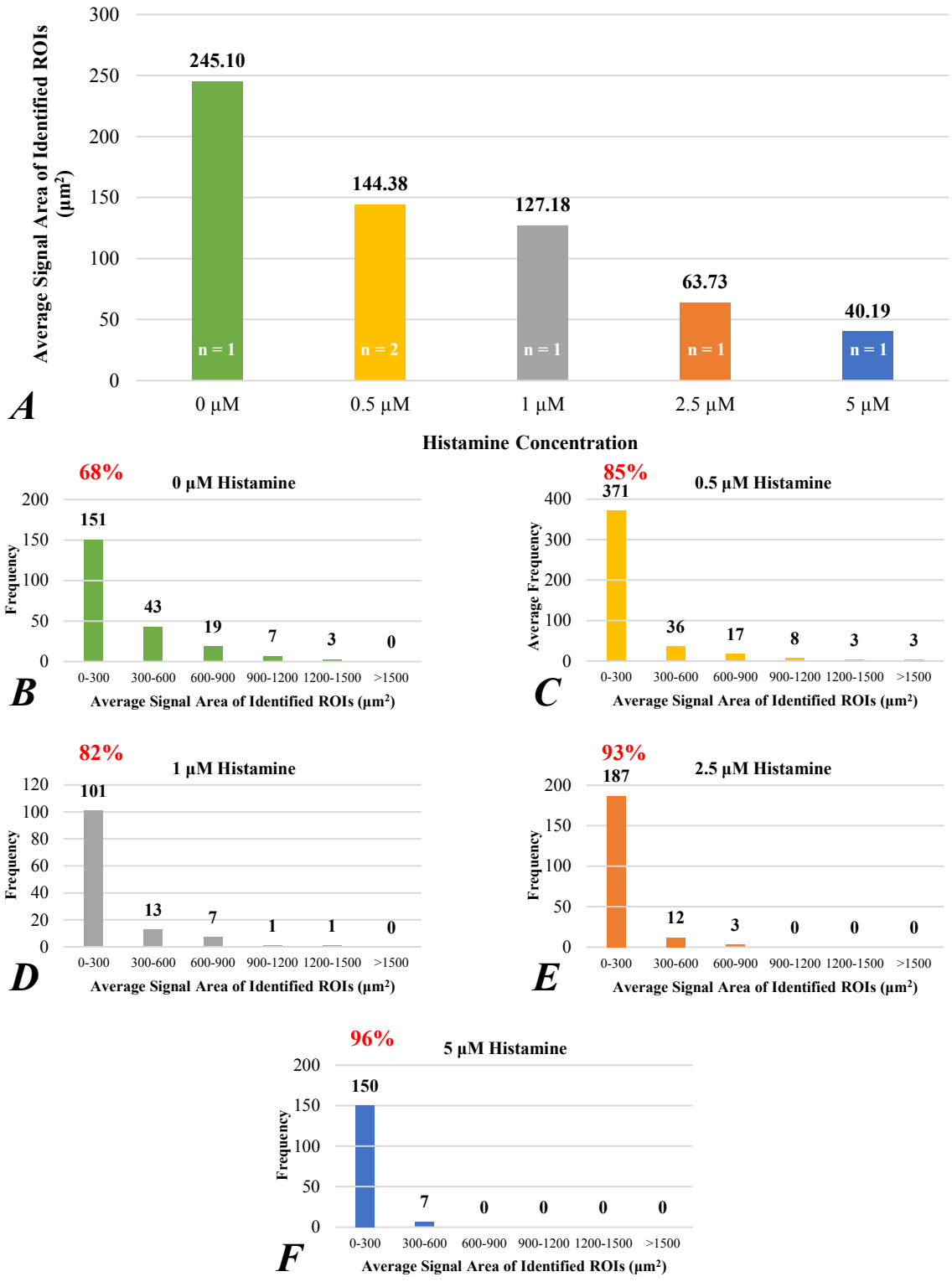

Figure 21. ***A*, Identified average signal area concentration-response curve generated from outputted S8 measurements for histamine. *B-F*, Frequency distributions for histamine.**

The average detected signal area values confirm the signals visualized in the processed images shown in Figures 16 and 19, where the detected Ca^{++} signal areas for the control experiment were ~70% greater than the responses at 0.5 μM as presented in Figure 21 panel *A*. There was also a 6-fold decrease in the average Ca^{++} signal area detected for the saturating concentration compared to the control as seen in Figure 21 panel *A*. However, this large decrease in Ca^{++} signal area with increasing histamine concentration could be due to the high baseline Ca^{++} activity of the control experiment observed in Figure 16. Otherwise, the average Ca^{++} signal areas decrease for increasing concentrations of histamine. Furthermore, for the 1 μM histamine treatment with an "n" of 2, the average signal areas for each experiment were ~118 and 171 μm^2, although their average peak intensities were markedly different.

The frequency distributions confirm what is seen in panel *A* of Figure 21 and illustrate that the percentage of smaller-area responses less than 300 μm^2 increases directly with concentration.

CHAPTER VII: CONCLUSION

Ca^{++} signals in ASM are critical for managing the contraction or relaxation of airways. When G_q agonists bind to G_q-coupled receptors, increases in cytosolic Ca^{++} consistently occur. Therefore, the goal of this project was to investigate if any spatial and kinetic differences in these Ca^{++} signals exist, which could explain the different airway responses to various G_q agonists. The novel S8 analysis software allowed quantitative measurements of these complex signals to be made. As explained in Chapter VI and as shown in Table 1, there were distinct spatial and kinetic differences in the induced Ca^{++} responses between the bitter taste agonist inducing relaxation, chloroquine, and contractile agonists carbachol and histamine. Although all 3 agonists are G_q-coupled, specific differences in the peak intensity, area, duration, and number of induced Ca^{++} signals were observed, which could potentially explain the distinct airway responses, either relaxation or contraction, in downstream studies. The average trends in these parameters were not only different for carbachol, chloroquine, and histamine, but some responses were concentration-dependent, and these responses did not follow a normal distribution. Specifically, chloroquine binding to the bitter taste receptor resulted in a possible bimodal, concentration-dependent response in the normalized average peak intensity that was not found with the other agonists.

Carbachol	Chloroquine	Histamine
Normalized Average Peak Intensity		
may not be concentration-dependent	*possibly concentration-dependent*	*possibly concentration-dependent*
negligible changes with increasing concentration (5 μM outlier): ~50% between 0 – 0.2	bimodal ~70% between 0 – 0.2 (except 10 μM)	no apparent changes on average For 0 μM: ~69% between 0 – 0.2 For 0.5 and 1 μM: ~35% between 0 – 0.2 For 2.5 and 5 μM: ~50% between 0 – 0.2
Average Signal Areas		
possibly concentration-dependent	*possibly concentration-dependent*	*possibly concentration-dependent*
~75% average increase from 1 to 50 μM ~85% < 300 μm^2 (5 μM outlier)	~137% average increase from 10 to 200 μM percentage of areas < 300 μm^2 decreases with increasing concentration	6-fold average decrease from 0 to 5 μM percentage of areas < 300 μm^2 approximately increases with increasing concentration
Average Signal Durations		
possibly concentration-dependent	*possibly concentration-dependent*	*possibly concentration-dependent*
~72% average increase from 0 to 50 μM 56 – 78% of responses are transient (0 – 40 s) or > 200 s (10 and 50 μM) majority of responses 0 – 40 s at lower concentrations (5 μM outlier)	~64% average increase from 0 to 200 μM ~42.5% between 0 – 40 s (0, 10, and 20 μM) ~22% between 0 – 40 s (100 and 200 μM)	~40% increase in average signal duration from 0 to 5 μM ~40% between 0 – 40 s (0 and 1 μM) ~50% between 0 – 40 s (2.5 and 5 μM)
Average Number of Identified Responses		
may not be concentration-dependent	*possibly concentration-dependent*	*possibly concentration-dependent*
~240 identified ROIs (5 μM outlier)	~71% average increase from 0 to 200 μM	~30% average decrease from 0 to 5 μM

Table 1. Average trends detected in the spatial and kinetic data obtained for the G_q receptor-coupled agonists carbachol, chloroquine, and histamine.

Future recommendations to advance this study include collecting more data to determine whether statistically significant differences occur. If the data are replicated, additional parameters can be analyzed and will possibly point to more spatial and kinetics differences between G_q agonists triggering relaxation or contraction of ASM, which could further support downstream studies linking these differences to the distinct airway responses. While four parameters were considered for this project, the S8 analysis software is a powerful tool that can also investigate Ca^{++} signals more deeply by measuring additional parameters over time, including the centroid of the area, the maximum area and

the time point it occurs, the change in intensity of a signal at each time point, the first frame time for each ROI, the starting location or coordinates of each signal ROI, the coordinates of the signal ROI at each time point and the intensity of each individual coordinate, and any convergence or divergence in the detected areas. Because bitter taste agonists are currently being explored as possible alternative or add-on treatments for asthma, studying Ca^{++} signal differences between relaxant and contractile G_q agonists with these additional signaling parameters coupled with the four studied in this project could be instrumental in determining implementation, especially if these responses are also concentration-dependent.

Additionally, because Ca^{++} mediates the relaxation or contraction of ASM, future studies could consider how these Ca^{++} signaling differences measured herein in response to the 3 different G_q agonists could affect the spread of mechanical forces. Lastly, future studies will involve measuring spatial and kinetic differences in induced intracellular Ca^{++} signals in HASMCs derived from asthmatic patients to determine if the observed responses are analogous to the responses presented in this thesis with HASMCs from a healthy donor.

REFERENCES

(1) An, S. S.; Bai, T. R.; Bates, J. H. T.; Black, J. L.; Brown, R. H.; Brusasco, V.; Chitano, P.; Deng, L.; Dowell, M.; Edelman, D. H.; Fabry, B.; Fairbank, N. J.; Ford, L. E.; Fredberg, J. J.; Gerthoffer, W. T.; Gilbert, S. H.; Gosens, R.; Gunst, S. J.; Halayko, A. J.; Ingram, R. H.; Irvin, C. G.; James, A. L.; Janssen, L. J.; King, G. G.; Knight, D. A.; Lauzon, A. M.; Lakser, O. J.; Ludwig, M. S.; Lutchen, K. R.; Maksym, G. N.; Martin, J. G.; Mauad, T.; McParland, B. E.; Mijailovich, S. M.; Mitchell, H. W.; Mitchell, R. W.; Mitzner, W.; Murphy, T. M.; Paré, P. D.; Pellegrino, R.; Sanderson, M. J.; Schellenberg, R. R.; Seow, C. Y.; Silveira, P. S. P.; Smith, P. G.; Solway, J.; Stephens, N. L.; Sterk, P. J.; Stewart, A. G.; Tang, D. D.; Tepper, R. S.; Tran, T.; Wang, L. Airway Smooth Muscle Dynamics: A Common Pathway of Airway Obstruction in Asthma. *Eur Respir J* **2007**, *29* (5), 834–860. https://doi.org/10.1183/09031936.00112606.

(2) Deshpande, D. A.; Wang, W. C. H.; McIlmoyle, E. L.; Robinett, K. S.; Schillinger, R. M.; An, S. S.; Sham, J. S. K.; Liggett, S. B. Bitter Taste Receptors on Airway Smooth Muscle Bronchodilate by Localized Calcium Signaling and Reverse Obstruction. *Nat Med* **2010**, *16* (11), 1299–1304. https://doi.org/10.1038/nm.2237.

(3) Conaway, S.; Nayak, A. P.; Deshpande, D. A. Therapeutic Potential and Challenges of Bitter Taste Receptors on Lung Cells. *Curr Opin Pharmacol* **2020**, *51*, 43–49. https://doi.org/10.1016/j.coph.2020.07.004.

(4) Rosenbaum, D. M.; Rasmussen, S. G. F.; Kobilka, B. K. The Structure and Function of G-Protein-Coupled Receptors. *Nature* **2009**, *459* (7245), 356–363. https://doi.org/10.1038/nature08144.

(5) GPCR | Learn Science at Scitable https://www.nature.com/scitable/topicpage/gpcr-14047471/ (accessed Mar 16, 2021).

(6) Billington, C. K.; Penn, R. B. Signaling and Regulation of G Protein-Coupled Receptors in Airway Smooth Muscle. *Respiratory Research* **2003**, *4* (1), 4. https://doi.org/10.1186/1465-9921-4-2.

(7) Ueda, T.; Ugawa, S.; Yamamura, H.; Imaizumi, Y.; Shimada, S. Functional Interaction between T2R Taste Receptors and G-Protein Alpha Subunits Expressed in Taste Receptor Cells. *J Neurosci* **2003**, *23* (19), 7376–7380.

(8) Pascoe, C. D.; Wang, L.; Syyong, H. T.; Paré, P. D. A Brief History of Airway Smooth Muscle's Role in Airway Hyperresponsiveness. *Journal of Allergy* **2012**, *2012*, e768982. https://doi.org/10.1155/2012/768982.

(9) Barisione, G.; Baroffio, M.; Crimi, E.; Brusasco, V. Beta-Adrenergic Agonists. *Pharmaceuticals (Basel)* **2010**, *3* (4), 1016–1044. https://doi.org/10.3390/ph3041016.

(10) Wendell, S. G.; Fan, H.; Zhang, C. G Protein–Coupled Receptors in Asthma Therapy: Pharmacology and Drug Action. *Pharmacol Rev* **2020**, *72* (1), 1–49. https://doi.org/10.1124/pr.118.016899.

(11) Nayak, A. P.; Shah, S. D.; Michael, J. V.; Deshpande, D. A. Bitter Taste Receptors for Asthma Therapeutics. *Front. Physiol.* **2019**, *10*. https://doi.org/10.3389/fphys.2019.00884.

(12) Abramson, M. J.; Walters, J.; Walters, E. H. Adverse Effects of Beta-Agonists: Are They Clinically Relevant? *Am J Respir Med* **2003**, *2* (4), 287–297. https://doi.org/10.1007/BF03256657.

(13) Sears, M. R. Adverse Effects of Beta-Agonists. *J Allergy Clin Immunol* **2002**, *110* (6 Suppl), S322-328. https://doi.org/10.1067/mai.2002.129966.

(14) BioRender https://app.biorender.com/gallery (accessed Apr 30, 2021).

(15) Gerthoffer, W. T. Agonist Synergism in Airway Smooth Muscle Contraction. *J Pharmacol Exp Ther* **1996**, *278* (2), 800–807.

(16) Katsunuma, T.; Roffel, A. F.; Elzinga, C. R.; Zaagsma, J.; Barnes, P. J.; Mak, J. C. Beta(2)-Adrenoceptor Agonist-Induced Upregulation of Tachykinin NK(2)

Receptor Expression and Function in Airway Smooth Muscle. *Am J Respir Cell Mol Biol* **1999**, *21* (3), 409–417. https://doi.org/10.1165/ajrcmb.21.3.3662.

(17) Mak, J. C.; Roffel, A. F.; Katsunuma, T.; Elzinga, C. R.; Zaagsma, J.; Barnes, P. J. Up-Regulation of Airway Smooth Muscle Histamine H(1) Receptor MRNA, Protein, and Function by Beta(2)-Adrenoceptor Activation. *Mol Pharmacol* **2000**, *57* (5), 857–864.

(18) Hill-Eubanks, D. C.; Werner, M. E.; Heppner, T. J.; Nelson, M. T. Calcium Signaling in Smooth Muscle. *Cold Spring Harb Perspect Biol* **2011**, *3* (9), a004549. https://doi.org/10.1101/cshperspect.a004549.

(19) Lock, J. T.; Parker, I.; Smith, I. F. A Comparison of Fluorescent Ca^{2+} Indicators for Imaging Local Ca2+ Signals in Cultured Cells. *Cell Calcium* **2015**, *58* (6), 638–648. https://doi.org/10.1016/j.ceca.2015.10.003.

(20) Tsien, R. Y. New Calcium Indicators and Buffers with High Selectivity against Magnesium and Protons: Design, Synthesis, and Properties of Prototype Structures. *Biochemistry* **1980**, *19* (11), 2396–2404. https://doi.org/10.1021/bi00552a018.

(21) Nelson, M.; Ledoux, J.; Taylor, M.; Bonev, A.; Hannah, R.; Solodushko, V.; Shui, B.; Tallini, Y.; Kotlikoff, M. Spinning Disk Confocal Microscopy of Calcium Signalling in Blood Vessel Walls. *Microsc Anal (Am Ed)* **2010**, *24* (2), 5–8.

(22) Francis, M.; Qian, X.; Charbel, C.; Ledoux, J.; Parker, J. C.; Taylor, M. S. Automated Region of Interest Analysis of Dynamic Ca^{2+} Signals in Image Sequences. *Am J Physiol Cell Physiol* **2012**, *303* (3), C236-243. https://doi.org/10.1152/ajpcell.00016.2012.

(23) Protocol for Loading Cal-520®, AM Into Live Cells | AAT Bioquest https://www.aatbio.com/resources/protocols/protocol-for-loading-cal-520-am-into-live-cells (accessed Apr 30, 2021).

(24) Schneider, C. A.; Rasband, W. S.; Eliceiri, K. W. NIH Image to ImageJ: 25 Years of Image Analysis. *Nature Methods* **2012**, *9* (7), 671–675. https://doi.org/10.1038/nmeth.2089.

(25) Gu, Q.; Lee, L.-Y. NEUROPHYSIOLOGY | Neural Control of Airway Smooth Muscle. In *Encyclopedia of Respiratory Medicine*; Laurent, G. J., Shapiro, S. D., Eds.; Academic Press: Oxford, 2006; pp 138–145. https://doi.org/10.1016/B0-12-370879-6/00253-2.
(26) Morgan, J. T.; Stewart, W. G.; McKee, R. A.; Gleghorn, J. P. The Mechanosensitive Ion Channel TRPV4 Is a Regulator of Lung Development and Pulmonary Vasculature Stabilization. *Cell Mol Bioeng* **2018**, *11* (5), 309–320. https://doi.org/10.1007/s12195-018-0538-7.

APPENDICES

Appendix A: Representative Experiments for S8-Processed Chloroquine Data

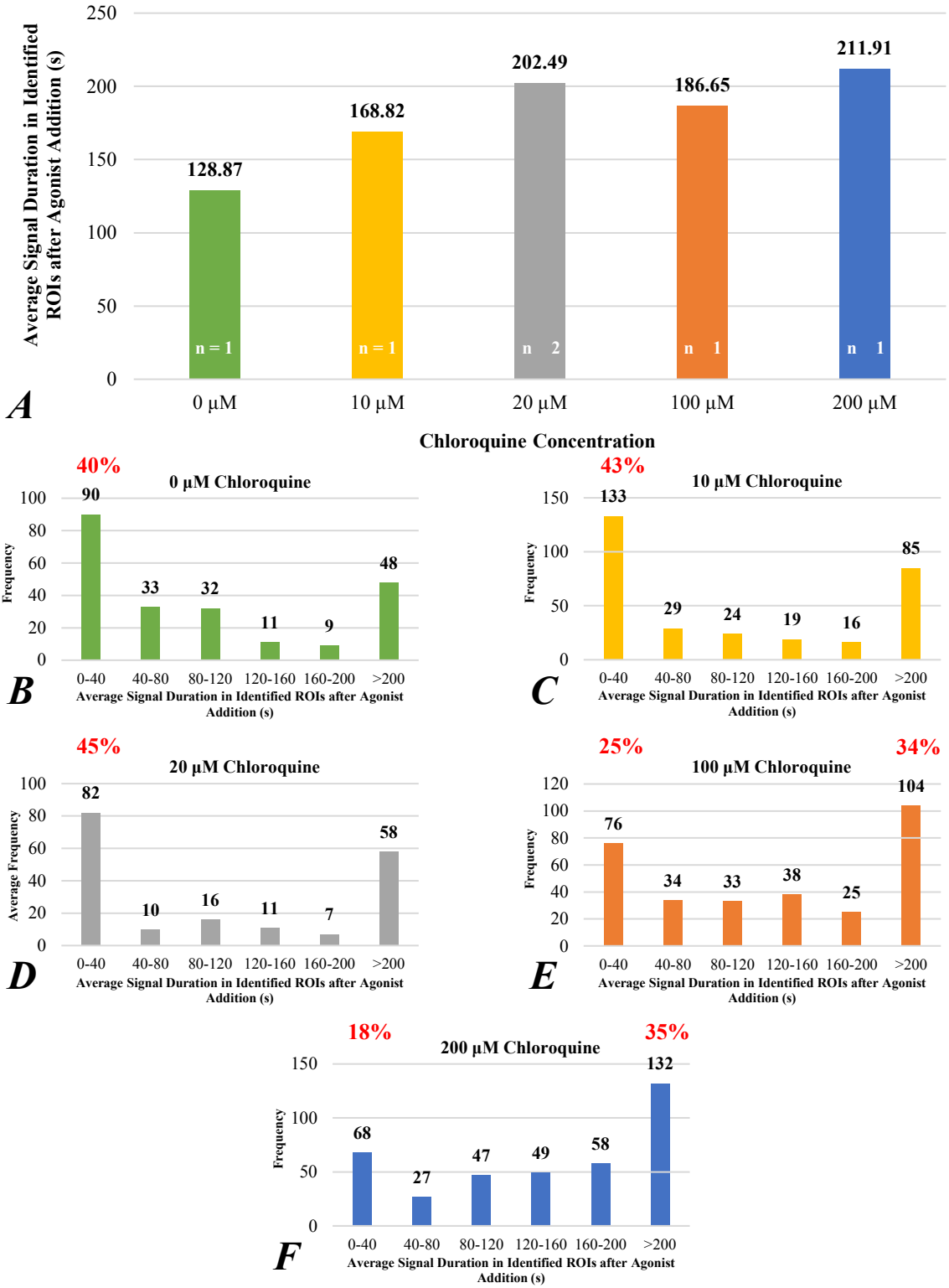

Figure A1. ***A*****, Average signal duration concentration-response curve generated from outputted S8 measurements for chloroquine.** ***B-F*****, Frequency distributions for chloroquine.**

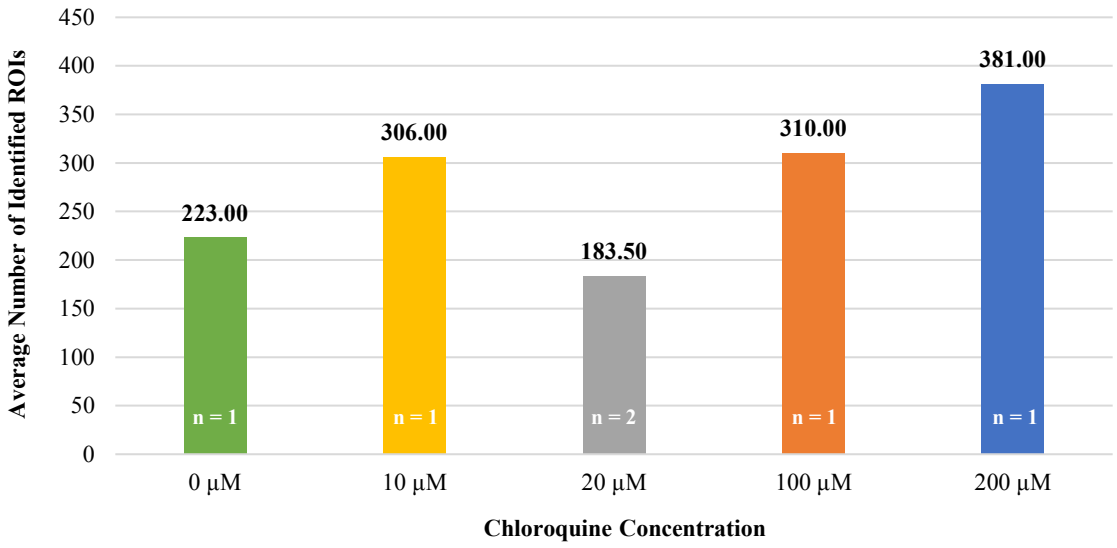

Figure A2. Average number of identified ROIs concentration-response curve generated from outputted S8 measurements for chloroquine.

Appendix B: Representative Experiments for S8-Processed Histamine Data

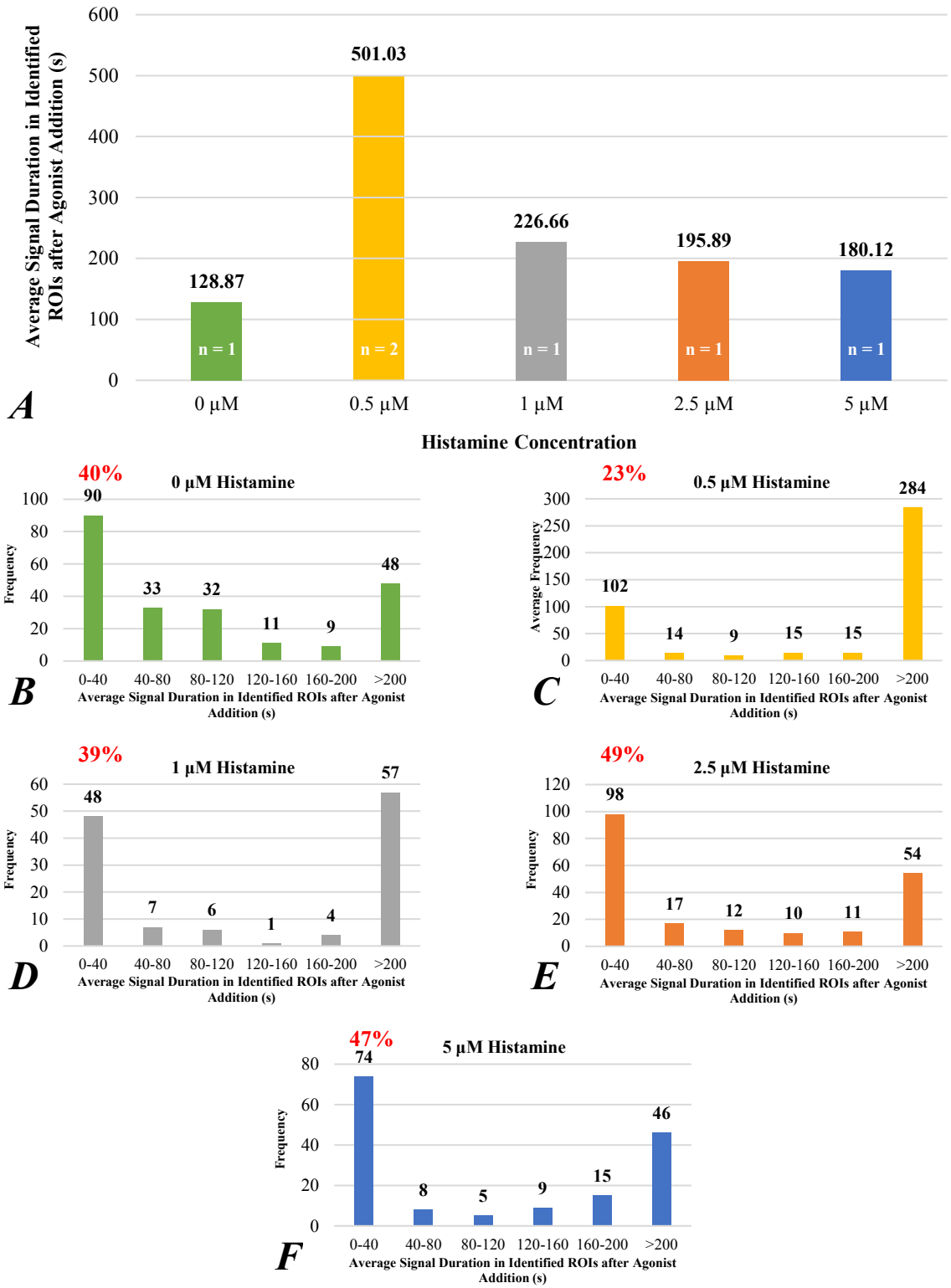

Figure B1. ***A*****, Average signal duration concentration-response curve generated from outputted S8 measurements for histamine.** ***B-F*****, Frequency distributions for histamine.**

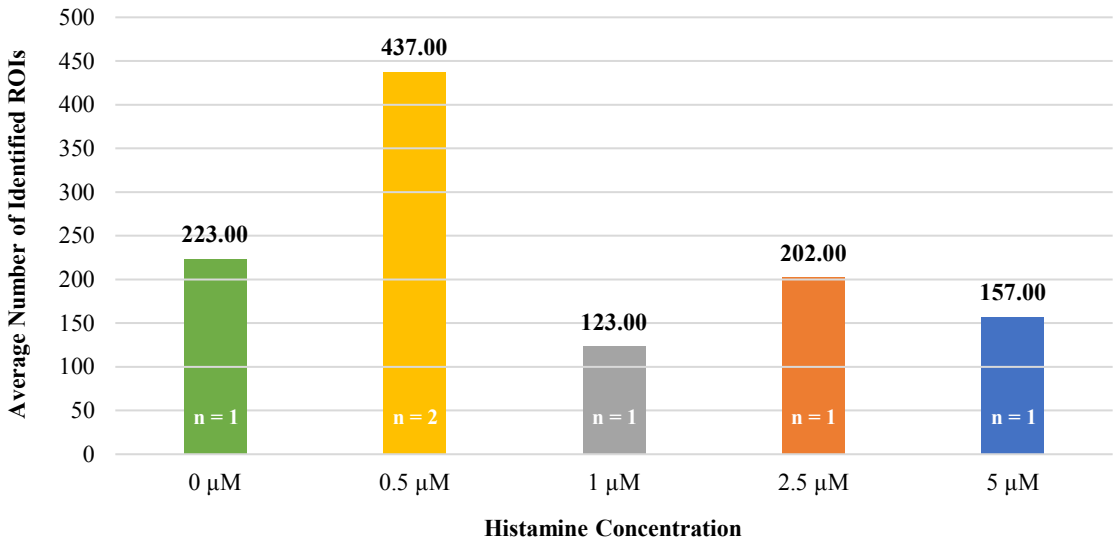

Figure B2. Average number of identified ROIs concentration-response curve generated from outputted S8 measurements for histamine.

BIOGRAPHICAL SKETCH

Name of Author: Hanna Viktoria Bobinger

Undergraduate School Attended:

University of South Alabama, Mobile, Alabama

Awards and Honors:

Mortar Board National Fellowship, 2021-22
American Heart Association Fellowship, 2018
Tau Beta Pi National Engineering Scholarship, 2020-21
University of South Alabama Academic All-Star 2018-21
Engineering Excellence Scholarship, 2017-2018

Publication:

Rich, T.; Southers, D. d.; Annamdevula, N. s.; Deal, J.; Bobinger, H.; Britain, A.; Francis, M.; Deshpande, D. a. Kinetics of Agonist-Induced Calcium Signals in Human Airway Smooth Muscle Cells. In *A30. CONTRACT AND RELAX: WHAT'S NEW IN AIRWAY SMOOTH MUSCLE MECHANISMS*; American Thoracic Society International Conference Abstracts; American Thoracic Society, 2020; pp A1258–A1258. https://doi.org/10.1164/ajrccm-conference.2020.201.1_MeetingAbstracts.A1258.